FINAL PROJECT REPORT #00042134-01-2D

GRANT: DTRT13-G-UTC45
Project Period: 05/30/17 – 05/30/19

Flexural Performance of Concrete Beams Strengthened using Different Repair Techniques

Participating Consortium Member:
Rutgers, The State University of New Jersey
New York University
Missouri University of Science and Technology

Authors:
Hani Nassif, P.E., Ph.D.
Professor and Associate Director
Adi Abu-Obeidah, Ph.D. Research Associate
Chaekuk Na, Ph.D. Senior Research Associate
Rutgers, The State University of New Jersey
Kaan Ozbay, Ph.D., Professor
Jingqin Gao, Ph.D. Candidate
New York University
Kamal Khayat, P.E., Ph.D.
Professor and Director
Missouri University of Science and Technology

RE-CAST:
REsearch on Concrete Applications for Sustainable Transportation
Tier 1 University Transportation Center

DISCLAIMER

TECHNICAL REPORT DOCUMENTATION PAGE

1. Report No. RECAST UTC #00042134-01-2D	**2. Government Accession No.**	**3. Recipient's Catalog No.**
4. Title and Subtitle Flexural Performance of Concrete Beams Strengthened using Different Repair Techniques		**5. Report Date** June 2019 **6. Performing Organization Code:**
7. Author(s) Hani Nassif, Adi Abu-Obeidah, Chaekuk Na, Kaan Ozbay, Jingqin Gao, Kamal Khayat		**8. Performing Organization Report No.** Project #00042134-01-2D
9. Performing Organization Name and Address RE-CAST - Rutgers, The State University of New Jersey 500 Bartholomew Road Piscataway, NJ 08854		**10. Work Unit No.** **11. Contract or Grant No.** USDOT: DTRT13-G-UTC45
12. Sponsoring Agency Name and Address Office of the Assistant Secretary for Research and Technology U.S. Department of Transportation 1200 New Jersey Avenue, SE Washington, DC 20590		**13. Type of Report and Period Covered:** Final Report Period: 05/01/2017 -05/01/2019 **14. Sponsoring Agency Code:**
15. Supplementary Notes The investigation was conducted in cooperation with the U. S. Department of Transportation.		

16. Abstract

With an aging infrastructure, the United States is faced with a wide variety of deterioration and lack of functionality for its bridges and highways. Economic factors do not always allow for a complete replacement of the structure which highlights the importance of the concrete rehabilitation technologies. Retrofitting existing structures using has fiber reinforced laminates shown to be effective and can increase the service life of the structure if applied properly. This study includes an experimental program of reinforced concrete beams retrofitted in flexure with fiber-reinforced ferrocement (FR-FC) and fiber-reinforced self-consolidating concrete (FR-SCC) laminates. The laminate acts as flexure reinforcement to the concrete structure element that suffered spalling and loss of concrete cover. In addition to FR-FC and FR-SCC, the use of unbonded tendons in prestressed concrete beams has been widely utilized in bridges, parking structures, and residential buildings for strengthening, rehabilitation or repair of such members. With the growth of live load and the increase of damaged concrete members, there is a need to develop and utilize new techniques for more efficient and improved designs in reinforced and prestressed concrete members. This research presents an experimental investigation to study the effect of the reinforcements, shear studs, depth of the concrete spalled and the fibers content in the CFRP tendons, FR-FC and FR-SCC laminate on the cracking load, ultimate capacity, deflection and the failure mode of the tested beams.

17. Key Words Bridge; repair; CFRP; Self-consolidating concrete; steel fibers; polypropylene fibers; ferrocement; Supplementary cementitious materials; Structural performance; Life cycle cost assessment.	**18. Distribution Statement** No restrictions. This document is available to the public.	
19. Security Classification (of this report) Unclassified	**20. Security Classification (of this page)** Unclassified	**21. No of Pages** 71

Form DOT F 1700.7 (8-72) Reproduction of form and completed page is authorized.

EXECUTIVE SUMMARY

With an aging infrastructure, the United States is faced with a wide variety of deterioration and lack of functionality for its bridges and highways. Economic factors do not always allow for a complete replacement of the structure which highlights the importance of the concrete rehabilitation technologies. Retrofitting existing structures using has fiber reinforced laminates shown to be effective and can increase the service life of the structure if applied properly. This study includes an experimental program of reinforced concrete beams retrofitted in flexure with fiber-reinforced ferrocement (FR-FC) and fiber-reinforced self-consolidating concrete (FR-SCC) laminates. The laminate acts as flexure reinforcement to the concrete structure element that suffered spalling and loss of concrete cover. In addition to FR-FC and FR-SCC, the use of unbonded tendons in prestressed concrete beams has been widely utilized in bridges, parking structures, and residential buildings for strengthening, rehabilitation or repair of such members.

With the growth of live load and the increase of damaged concrete members, there is a need to develop and utilize new techniques for more efficient and improved designs in reinforced and prestressed concrete members. This research presents an experimental investigation to study the effect of the reinforcements, shear studs, depth of the concrete spalled and the fibers content in the CFRP tendons, FR-FC and FR-SCC laminate on the cracking load, ultimate capacity, deflection and the failure mode of the tested beams.

Keywords:

Bridge; repair; CFRP; Self-consolidating concrete; steel fibers; polypropylene fibers; ferrocement; Supplementary cementitious materials; Structural performance; Life cycle cost assessment.

ACKNOWLEDGEMENT

The authors would like to acknowledge the many individuals and organizations that made this research project possible. First and foremost, the authors would like to acknowledge the financial support of Missouri Department of Transportation (MoDOT) as well as the RE-CAST (REsearch on Concrete Applications for Sustainable Transportation) Tier-1 University Transportation Center (UTC) at Missouri University of Science and Technology (Missouri S&T).

The authors would also like to thank the companies that provided materials required for the successful completion of this project, including LafargeHolcim, BASF, Euclid Chemical, Buildex, and Capital Sand Company, as well as Granuband Macon.

The cooperation and support from Abigayle Sherman and Gayle Spitzmiller of the Center for Infrastructure Engineering Studies (CIES) are greatly acknowledged, in particular the assistance of Dr. Soo-Duck Hwang, Lead Scientist, and Jason Cox, Senior Research Specialist is highly appreciated. Valuable technical support provided by technical staff of the Department of Civil, architectural, and Environmental Engineering at Missouri S&T is deeply appreciated, in particular Brian Smith, John Bullock, and Gary Abbott.

Table of Contents

EXECUTIVE SUMMARY i
ACKNOWLEDGEMENT ii
Table of Contents iii
List of Figures v
List of Tables vi
1. INTRODUCTION 1
1.1. Problem Statement 1
1.2. Research Objectives 2
1.3. Research Methodology 2
2. EXPERIMENTAL PROGRAM 3
2.1. Materials 3
2.2. Testing Program 5
2.2.1. Mix Design Proportions 5
2.3. Mixing Procedure 10
2.3.1. Fiber Reinforced Ferrocement (FR-FC) 10
2.3.2. Concrete Mixtures 11
2.4. Test Methods 11
2.4.1. Test Methods for Mortar Mixtures 11
2.4.2. Test Methods for Concrete Mixtures 12
3. CONCRETE PERFORMANCE EVALUATION 14
3.1. Fresh Properties 14
3.1.1. Test Methods for Concrete Mixtures 14
3.1.2. T20 and Visual Stability Index (VSI) 14
3.1.3. Air Content 15
3.2. Mechanical Properties 15
3.2.1. Fiber Reinforced Self-Consolidating Concrete (FR-SCC) 15
3.2.2. Fiber Reinforced Ferrocement (FR-FC) 16
3.3. Free Shrinkage properties 18
3.3.1. Fiber Reinforced Self-Consolidating Concrete (FR-SCC) 18
3.3.2. Fiber Reinforced Ferrocement (FR-FC) 19
4. BEAM TESTING DETAILS AND RESULTS 20
4.1. Structural Performance of Concrete Beams Repaired with FR-SCC and FR-FC 20

4.1.1. Specimens Preparation 20
4.1.2. Results of FR-SCC and FR-FC Reinforced Concrete Beams 24
4.1.3. Comparison of FR-SCC and FR-FC Reinforced Concrete Beams 31
4.2. Structural Performance of Prestressed Concrete Beams with Hybrid Tendons 33
4.2.1. Specimens Preparation 33
4.2.2. Hybrid Beams Testing Results 37
5. LIFE CYCLE COST ANALYSIS 43
5.1. Introduction 43
5.2. Literature Review 43
5.3. Stochastic Multi-Objective Optimization-based LCCA Framework 46
5.3.1. Project-level LCCA Model 47
5.3.2. Network-Level Multi-Objective Optimization Model 48
5.4. Structure Considered 50
5.4.1. Hypothetical Project-level LCCA Example 52
5.4.2. Hypothetical Network-level LCCA Example 55
6. SUMMARY AND CONCLUSIONS 59
6.1. FR-SCC and FR-FC Strengthened Beams 59
6.2. Hybrid Prestressed Beams 59
6.3. LCCA 60
REFERENCES 61

List of Figures

Figure 2.1. Mortar Mixer 11
Figure 3.1. Free Shrinkage Strain (μs) vs Time (Days) for FR-SCC Mixes 18
Figure 4.1. Specimen Dimensions; (a) Beam Set Number 1 & 2 and (b) Beam Set Number 3 & 4 20
Figure 4.2. Install Laminates Prior to Casting Repair Material 21
Figure 4.3. Small Beam Testing Setup 21
Figure 4.4. Load-Deflection Response for FR-SCC Beams, (a) Compared to Control Beams and (b) Effect of Fibers Only 25
Figure 4.5. Load-Deflection Response, (a) H1 Mixes, (b) H2 Mixes, (c) P2 Mixes 26
Figure 4.6. Load-Deflection Response, (a) 8 Layers, (b) 5 Layers 27
Figure 4.7. Cracking Performance of FR-SCC Specimens (SCC) 28
Figure 4.8. Load-Deflection Response for FR-FC Beams, (a) Compared to Control Beams and (b) Effect of Fibers Only 28
Figure 4.9. Load-Deflection Response, (a) H1 Mix, (b) H2 Mix, (c) 0.1 & 0.2% Fiber Mix 29
Figure 4.10. Load-Deflection Response, (a) 8 Layers, (b) 5 Layers 30
Figure 4.11. Cracking Performance of FR-FC Specimens (FC) 31
Figure 4.12. Load-Deflection Response for FR-SCC vs FR-FC 32
Figure 4.13. Experimental Program Plan Chart 33
Figure 4.14. Steel Anchorage Jacking using Aslan 250 Tendons 34
Figure 4.15. Beam Design and Cross Section Details; (a) Beam Design, (b) Hybrid Beam Cross Section, and (c) Unbonded Beam Cross Section 35
Figure 4.16. Overview of Loading Frame and Strain Measuring Instruments Locations 36
Figure 4.17. Effect of Bonded Tendons Area on Load-Deflection Behavior for Same Unbonded Tendon; (a) A_{psu} = 0.085 in^2, (b) A_{psu} = 0.153 in^2, (c) A_{psu} = 0.11 in^2 39
Figure 4.18. Effect of Unbonded Tendons Area (Hybrid Beams) on Load-Deflection Behavior for Same Bonded Tendon (a) A_{psb} = 0.085 in^2, (b) A_{psb} = 0.153 in^2 40
Figure 4.19. Effect of Unbonded Tendons Area (Unbonded Beams) on Load-Deflection Behavior 40
Figure 4.20. Effect of Unbonded Tendons Material (Steel/FRP) on Load-Deflection Behavior; (a) d_{psb} = 8.875 in, d_{psu} = 6.125 in, (b) d_{psb} = 7.5 in, d_{psu} = 8.875 in 41
Figure 4.21. Effect of Tendons Depth (Both Bonded and Unbonded) on Load-Deflection Behavior (a) Steel Tendons, (b) CFRP Tendons 41
Figure 4.22. Effect of Hybrid Combination Compared to Fully Bonded and Unbonded on Load-Deflection Behavior 42
Figure 4.23. Effect of Beam Length on Load-Deflection Behavior 42
Figure 5.1. An integrated project- and network-level LCCA model framework. 46
Figure 5.2. PDF and CDF Plots for Project-Level LCCA; (a) PDF and CDF for Agency Cost and (b) PDF and CDF for Weighted Life Cycle Cost 53
Figure 5.3. Network-Level Optimization Model Results 56
Figure 5.4. Strategy 1: Maximizing Available Budget; (a) Conventional and (b) FR-FC+FR-SCC (+10) 57
Figure 5.5. Strategy 2: Maximizing Network Condition Ratings; (a) Conventional and (b) FR-FC+FR-SCC (+10) 57

List of Tables

Table 2.1. Materials and Suppliers 3
Table 2.2. Coarse and Fine Aggregate Properties........ 4
Table 2.3. Fiber Properties........ 4
Table 2.4. CFRP Tendon Properties 4
Table 2.5. FR-SCC Mixture Proportions 5
Table 2.6. FR-FC Mixture Proportions of Mortar Group 1 6
Table 2.7. FR-FC Mixture Proportions of Mortar Group 2 7
Table 2.8. FR-FC Mixture Proportions of Mortar Group 3 8
Table 2.9. FR-FC Mixture Proportions of Mortar Group 4 9
Table 2.10. HPC Mixture Proportions 10
Table 2.11. Class A Mixture Proportions 10
Table 3.1. Slump Flow Values and J-Ring Test Results........ 14
Table 3.2. T20 and VSI Test Results 15
Table 3.3. Air Content Test Results........ 15
Table 3.4. Mechanical Properties (% difference compared to the control mix, PPF 0.00) 16
Table 3.5. Mix Design for Base Mortar Mix 16
Table 3.6. Fiber Content of Each Mortar Mix Group 17
Table 3.7. Mechanical Properties of FR-FC 17
Table 3.8. Shrinkage Properties 18
Table 3.9. Free Shrinkage Strain of FR-FC 19
Table 4.1. FR-SCC Testing Program 22
Table 4.2. FR-FC Testing Program........ 23
Table 4.3. FR-SCC Testing Results 24
Table 4.4. FR-FC Testing Results 25
Table 4.5. FR-SCC Cracking Performance Results........ 27
Table 4.6. FR-FC Cracking Performance Results 30
Table 4.7. FR-FC vs FR-SCC Cracking Performance Results 32
Table 4.8 Mechanical Properties of CFRP Tendons (Hughes Brothers) 34
Table 4.9. Summary of Beam Properties and Parameters (f'c= 12 ksi, ds = 9 in, As = 0.22 in^2). 35
Table 4.10. Overview of Each Sensors Details and Purpose 36
Table 4.11. Summary of Applied and Measured Mid-Span Deflections at Various Limit States 38
Table 5.1. Literature Review on Network-level Life Cycle Cost Models 45
Table 5.2. National Bridge Inventory Code Item 43 - Structure Type, Main (Administration 1995) 50
Table 5.3. AASHTO LRFD Table 2.5.2.6.3-1 Traditional Minimum Depths for Constant Depth Superstructures........ 51
Table 5.4. Project-Level LCCA Inputs 54
Table 5.5. Project-Level LCCA Results 54
Table 5.6. Cost Difference Compare with Conventional Repair Approach 54
Table 5.7. Bridges Selected for Network-Level LCCA Analysis........ 55
Table 5.8. Clusters based on Maximizing Network Condition Rating and Available Budget – Top Solution in Each Cluster 58

1. INTRODUCTION

1.1. Problem Statement

The deteriorated state of the current infrastructure is problematic and economic factors limit the complete replacement of structures, stressing the importance on rehabilitation to extend the life of existing structures. Our infrastructure relies on old bridges, buildings, dams, etc. which produce a massive economic strain in the form of repair and maintenance. Tearing down an old structure to create a new one is not nearly as economical as its improvement or repair. Most of our concrete infrastructure is older than 20 years, and the national grand challenge of maintenance and repair is well-known. Approximately 68.5% of all the U.S. bridges are older than 25 years old and 30.8% are over 50 years old (ASCE, 2017). In the area of bridges alone, according to the U.S. National Bridge Inventory (2013), there are over 605,000 bridges of which 11.7% are functionally obsolete and 14.7% are structurally deficient. These economic factors force our hands as engineers to produce new technologies to increase economic efficiency. Therefore, the aim of this project is to develop and validate the use of new advanced cementitious materials to improve the flexural capacity of reinforced concrete beams to extend their service life. Among various new technologies, the team will focus on the following materials, fiber reinforced ferrocement (FR-FC), fiber reinforced self-consolidating concrete (FR-SCC) and carbon fiber reinforced polymer tendons (CFRP)

Ferrocement (FC) and self-consolidating concrete (SCC) have gained a lot of traction in its usefulness for repairing and retrofitting due to its ease of application and bond strength to the applied substrate. The proposed project will develop the FR-SCC and FR-FC mix proportions that involve several cementitious materials, fibers types and dosages. Afterwards, optimum mixtures will be tested on the soffit of damaged reinforced concrete beams to evaluate the improvement in the flexural capacity of the structure member.

Similarly, the CFRP has been gaining a lot of attention in prestressed members' applications due to its high corrosion resistance and light weight. In addition, it exhibits linear stress-strain relationship resulting in more accurate predictions for the tendon stress at ultimate. CFRP tendons are utilized in this project as a unbonded tendons in pre-tensioned concrete member (hybrid beam). With the availability of high strength concrete, as well as the development of new prestressing technologies, the process can be easily performed at the site for repair or capacity upgrading resulting in longer spans for the same section depth or shallower sections. There is a knowledge gap on the behavior of concrete beams prestressed with hybrid tendons and a need to fully understand their overall behavior under full service loads. This investigation included the testing of 15 high strength concrete (HSC) beams prestressed with hybrid tendons at different depths and diameters.

1.2. Research Objectives

The specific objectives of this project are described as follows:

- Comparing the effectiveness of different innovative materials, including slag (SL), fly ash (FA), silica fume (SF), synthetic polypropylene fiber (PPF) and steel fiber (STF) when added to SCC and FC mix proportions to improve resistance to cracking.
- Developing new classes of FR-SCC and FR-FC materials with high cracking resistance, and appropriate slump consistencies targeted for transportation infrastructure repair and retrofitting applications.
- Analysis and comparison of the strength and shrinkage properties between FR-SCC and FR-FC. Enormous efforts have been made to develop such mixes by optimizing the mixture design or adding various types of fibers.
- Conducting an experimental program with T-beams prestressed with unbonded CFRP with steel tendons and hybrid tendons (steel with CFRP or bonded with unbonded tendons).
- As a part of the RE-CAST research, an attempt was also made to develop a systematic workflow and guidelines for comparing the life cycle cost of conventional and new construction materials or technologies to assist decision-makers in finding optimum strategies with the ultimate goal of maintaining components of our transportation infrastructure such as pavements and bridges, in safe and efficient condition over time.

1.3. Research Methodology

The research project includes three tasks as presented below, while Task 1 and Task 2 were performed by Rutgers University and Task 3 was performed by New York University with the help of Rutgers University:

Task 1 – Investigation on Mechanical Properties of Innovative Materials

A comprehensive investigation was undertaken to evaluate the influence of mixture proportioning (FR-SCC and FR-FC) and material characteristics on various properties, including workability, mechanical properties, shrinkage, and durability.

Task 2 – Small- and Large-Scale Beam Testing using Innovative Materials

Small and Large-scale reinforced concrete specimens were constructed to evaluate flexural performance of the repaired beams. Small-scale beams were utilized with the FR-SCC and FR-FC mixtures and large-scale beams were utilized with CFRP tendons.

Task 3 - Life Cycle Assessment

Life-cycle evaluation of our transportation infrastructures is one of the crucial steps to achieving sustainable transportation and it becomes more important as technical and environmental needs grow and new repair and rehabilitation materials or technologies are developed. However, it remains a challenge to track the acceptance of the new construction materials or technologies and to reliably estimate their lifetime performance due to limited data. To address these issues, the proposed approach with stochastic treatment allows us to probabilistically evaluate new materials or technologies using a metaheuristic evolutionary algorithm while satisfying project- and network-wide constraints. The proposed methodology provides an effective solution to many issues that have not been completely addressed in the past, including the trade-off between multiple objectives, effect of time, uncertainty and outcome interpretation.

2. EXPERIMENTAL PROGRAM

2.1. Materials

This chapter describes constituent materials, testing program, mixing procedure, and method employed for this research program. Materials were obtained from various local suppliers in NJ and Eastern PA. Both fine and coarse aggregates were obtained from Clayton Concrete plant in Edison, NJ. Grade 120 slag cement and Type I Portland cement were supplied by LaFarge-Holcim in Camden, NJ and Whitehall, PA, respectively. The chemical admixtures as well as micro and macro synthetic polypropylene (PPF) fibers were provided by Euclid Chemical in East Brunswick, NJ. The list of suppliers of each material is summarized in Table 2.1.

Type I Portland cement is tested by the manufacturer to comply with all the requirements set by ASTM C150 including chemical composition, physical properties, reactivity and strength requirements. Similar requirements are outlined in ASTM C989 for the slag cement used. Manufacturer testing assures that Grade 120 slag cement meets the reactivity and other requirements set by ASTM standards.

Table 2.1. Materials and Suppliers

Material	Type	Supplier
Cement	Portland Type I	LaFarge-Holcim
Slag cement	Grade 120	LaFarge-Holcim
Fly Ash	Class F	Titan America
Fine aggregate	Concrete Sand	Clayton Concrete
Coarse aggregate	#8 (3/8 in.) granite	Clayton Concrete
Macro Synthetic Fibers	Polypropylene (2, 1.5, 3/4 and 1/4 in.)	Euclid Chemical
Crimped Steel Fiber	1.5 in	Euclid Chemical
High Range Water Reducer	Plastol 5000	Euclid Chemical
Air Entraining Agent	AEA-92S	Euclid Chemical

Sieve analyses on both types of aggregate were performed according to ASTM C136. Coarse aggregate properties, including density, specific gravity, and absorption were determined using the procedure outlined in ASTM C127. The properties of sand were determined using ASTM C128. The results of these tests are summarized in Table 2.2.

Table 2.2. Coarse and Fine Aggregate Properties

Properties	Fine aggregate	Coarse aggregate
Specific gravity (unit-less)	2.62	2.83
Fineness modulus (unit-less)	2.35	6.03
Absorption (%)	1.10	0.40

The micro and macro synthetic polypropylene fibers and steel fibers used in this study comply with ASTM C1116 and ASTM D7508. The properties of the fibers provided by the manufacturer are summarized in Table 2.3.

Table 2.3. Fiber Properties

Material	Micro Synthetic Fiber	Macro Synthetic Fiber	Crimped Steel Fiber
Specific gravity (unit-less)	0.91	0.92	NA
Length (mm, in.)	6.4 (1/4)	19 (3/4), 38 (1.5), 50 (2)	38 (1.5)
Melting point (°C, °F)	160 (320)		NA
Denier	15		NA

Aslan 250 tendons are utilized in this study. These tendons are typically used to strengthening existing structural member in flexure and shear. As stated by the manufacturer, Structures that are deficient due to either a structural flaw, deterioration or because of a change in use can often be brought to a useful capacity using Aslan 200 series CFRP. The properties of the CFRP tendons are provided by the manufacturer are summarized in Table 2.4.

Table 2.4. CFRP Tendon Properties

Material	Aslan 250 - #3	Aslan 250 - #4
Nominal Diameter (in)	3/8	1/2
Nominal Area (in2)	0.11	0.196
Ultimate tensile load (kips)	34.65	58.8
Tensile modulus of elasticity (Ef)	18	18
Ultimate Strain (%)	1.75	1.67

2.2. Testing Program

2.2.1. Mix Design Proportions

Fiber Reinforced Self-Consolidating Concrete (FR-SCC)

A total of eight (8) fiber-reinforced concrete mixtures were prepared for this experimental study. The proportions of these mixtures are based primarily on the findings of a previous study conducted by the Virginia Transportation Research Council (Brown et al., 2010). All samples for each mixture were cast from a single batch to ensure uniformity. The mixture proportions are summarized in Table 2.5. In an effort to isolate variables, mixture proportions were kept identical in all four mixtures except fiber content. Each mixture contains 400 kg/m^3 (675 lb./yd^3) of total cementitious material, 35% of which is Grade 120 slag cement and 65% of which is Type I Portland cement. A water-to-cementitious ratio (w/cm) of 0.425 is targeted with a tolerance of ± 0.02. Equal amounts of coarse and fine and aggregates of 852 kg/m^3 (1,436 lb/yd^3) were used in each mixture, and the coarse-to-fine aggregate ratio is 1-to-1.

Table 2.5. FR-SCC Mixture Proportions

Mixture ID	PPF 0.00	PPF1 0.30	PPF1 0.50	PPF2 0.30	PPF3 0.30	STF2 0.20	STF2 0.50	HPPF1 0.11	HSTF2 0.16
Type I Portland (kg/m^3, lb/yd^3)	260 (439)	260 (439)	260 (439)	260 (439)	260 (439)	260 (439)	260 (439)	260 (439)	260 (439)
Grade 120 slag (kg/m^3, lb/yd^3)	140 (236)	140 (236)	140 (236)	140 (236)	140 (236)	140 (236)	140 (236)	140 (236)	140 (236)
Total cementitious material (kg/m^3, lb/yd^3)	400 (675)	400 (675)	400 (675)	400 (675)	400 (675)	400 (675)	400 (675)	400 (675)	400 (675)
W/C ratio	0.425	0.425	0.425	0.425	0.425	0.425	0.425	0.425	0.425
#8 Rock (kg/m^3, lb/yd^3)	852 (1436)	852 (1436)	852 (1436)	852 (1436)	852 (1436)	852 (1436)	852 (1436)	852 (1436)	852 (1436)
Fine aggregate (kg/m^3, lb/yd^3)	852 (1436)	852 (1436)	852 (1436)	852 (1436)	852 (1436)	852 (1436)	852 (1436)	852 (1436)	852 (1436)
HRWR (kg/m^3, oz./yd^3)	2.5 (68)	3 (81)	3 (81)	3.5 (95)	3.5 (95)	3.5 (95)	3 (81)	3.5 (95)	3.5 (95)
Macro Fiber (PPF) vol% & Length (in)	-	0.3% 0.75 in	0.5% 0.75 in	0.3% 1.5 in	0.3% 2.0 in	-	-	-	0.15% 0.75 in
Micro Fibers (PPF) vol% & Length (in)	-	-	-	-	-	-	-	0.01% 0.75 in	0.01% 0.75 in
Steel Fibers (STF) vol% & Length (in)	-	-	-	-	-	0.2% 1.5 in	0.5% 1.5 in	0.1% 1.5 in	-

This research was carried out using steel crimped fibers (STF), micro and macro polypropylene fibers (PPF). Fiber volume was varied between mixtures, beginning with the control mixture (PPF 0.00) having no fibers and other mixtures having 0.11%, 0.16%, 0.20%, 0.3% and 0.5% fiber by volume. As the addition of fibers resulted in lower workability, additional HRWR was added to the batch until the desired workability and flowability were met. The control mixture included 2.5 kg/m3 (68 fl. oz./yd3) of HRWR, while fiber reinforced mixtures contained 3 kg/m3 (81 fl. oz./yd3) to 3.5 kg/m3 (95 fl. oz./yd3) of HRWR.

Fiber Reinforced Ferrocement (FR-FC)

The experimental work performed for this study included 22 different mortar mixes divided in 4 groups. Various combinations of cementitious materials, different fiber types and lengths were used in order to find the optimal mixes for repair purposes. The mixtures investigated are summarized in Table 2.6 through Table 2.9. Among these mixes, the team promoted several selected mixes in Group 1, Group 2 and Group 3 for beam testing.

Table 2.6. FR-FC Mixture Proportions of Mortar Group 1

Mixture ID	C1	C1PPF	C1STF
Type I Portland cement (kg/m3, lb/yd3)	648 (1095)	648 (1095)	648 (1095)
Grade 120 slag cement (kg/m3, lb/yd3)	-	-	-
Fly Ash (kg/m3, lb/yd3)	-	-	-
Silica fume (kg/m3, lb/yd3)	-	-	-
Total cementitious material (kg/m3, lb/yd3)	648 (1095)	648 (1095)	648 (1095)
W/C ratio	0.4	0.4	0.4
Fine aggregate/Sand (kg/m3, lb/yd3)	1296 (2190)	1296 (2190)	1296 (2190)
HRWR (kg/m3, oz./yd3)	2 (54)	2 (54)	2 (54)
Shrinkage Reducing Admixture (gal./yd3)	1	1	1
Macro Fiber (PPF) vol% & Length (in)	-	0.1% 0.75 in.	-
Micro Fibers (PPF) vol% & Length (in)	-	-	-
Steel Fibers (STF) vol% & Length (in)	-	-	0.1% 0.75 in.
C1: Group one control mix PPF: Macro Synthetic Fiber (PPF) STF: Steel Fiber			

Table 2.7. FR-FC Mixture Proportions of Mortar Group 2

Mixture ID	C2	C2PPF	C2STF	C2PPF1	C2PPF2	C2PPF3	C2H1	C2H2
Type I Portland (kg/m3, lb/yd3)	615 (1040)	615 (1040)	615 (1040)	615 (1040)	615 (1040)	615 (1040)	615 (1040)	615 (1040)
Grade 120 slag (kg/m3, lb/yd3)	-	-	-	-	-	-	-	-
Fly Ash (kg/m3, lb/yd3)	-	-	-	-	-	-	-	-
Silica fume (kg/m3, lb/yd3)	33 (55)	33 (55)	33 (55)	33 (55)	33 (55)	33 (55)	33 (55)	33 (55)
Total cementitious material (kg/m3, lb/yd3)	648 (1095)	648 (1095)	648 (1095)	648 (1095)	648 (1095)	648 (1095)	648 (1095)	648 (1095)
W/C ratio	0.4	0.4	0.4	0.4	0.4	0.4	0.4	0.4
Fine aggregate/Sand (kg/m3, lb/yd3)	1296 (2190)	1296 (2190)	1296 (2190)	1296 (2190)	1296 (2190)	1296 (2190)	1296 (2190)	1296 (2190)
HRWR (kg/m3, oz./yd3)	2 (54)	2 (54)	2 (54)	4 (108)	4 (108)	4 (108)	4 (108)	4 (108)
Shrinkage Reducing Admixture (gal./yd3)	1	1	1	1	1	1	1	1
Macro Fiber (PPF1) vol% & Length (in)	-	0.2% 0.75 in.	-	0.1% 0.75 in.	-	-	0.1% 0.75	-
Macro Fiber (PPF2) vol% & Length (in)	-	-	-	-	0.1% 1.5 in.	-	0.1% 1.5	0.1% 1.5
Macro Fiber (PPF3) vol% & Length (in)	-	-	-	-	-	0.1% 2.0 in.	-	-
Micro Fibers (PPF) vol% & Length (in)	-	-	-	-	-	-	-	-
Steel Fibers (STF) vol% & Length (in)	-	-	0.1% 0.75 in.	-	-	-	-	0.1% 0.75

C2: Group two control mix
H: Hybrid between two types of fiber
PPF1: Macro Synthetic Fiber (PPF) – length = 0.75"
PPF2: Macro Synthetic Fiber (PPF) – length = 1.5"
PPF3: Macro Synthetic Fiber (PPF) – length = 2.0"

Table 2.8. FR-FC Mixture Proportions of Mortar Group 3

Mixture ID	C3	C3PPF	C3STF
Type I Portland (kg/m^3, lb/yd^3)	517 (874)	517 (874)	517 (874)
Grade 120 slag (kg/m^3, lb/yd^3)	-	-	-
Fly Ash (kg/m^3, lb/yd^3)	97 (164)	97 (164)	97 (164)
Silica fume (kg/m^3, lb/yd^3)	33 (55)	33 (55)	33 (55)
Total cementitious material (kg/m^3, lb/yd^3)	648 (1095)	648 (1095)	648 (1095)
W/C ratio	0.4	0.4	0.4
Fine aggregate/Sand (kg/m^3, lb/yd^3)	1296 (2190)	1296 (2190)	1296 (2190)
HRWR (kg/m^3, lb/yd^3)	2 (54)	2 (54)	2 (54)
Shrinkage Reducing Admixture ($gal./yd^3$)	1	1	1
Macro Fiber (PPF) vol% & Length (in)	-	0.1% 0.75 in	-
Micro Fibers (PPF) vol% & Length (in)	-	-	-
Steel Fibers (STF) vol% & Length (in)	-	-	0.1% 0.75 in.
C3: Group three control mix PPF: Macro Synthetic Fiber (PPF) STF: Steel Fiber			

Table 2.9. FR-FC Mixture Proportions of Mortar Group 4

Mixture ID	C4	C4PPF1	C4PPF2	C4PPF3	C4STF	C5	C5PPF	C5STF
Type I Portland (kg/m^3, lb/yd^3)	517 (874)	517 (874)	517 (874)	517 (874)	517 (874)	517 (874)	517 (874)	517 (874)
Grade 120 slag (kg/m^3, lb/yd^3)	97 (164)	97 (164)	97 (164)	97 (164)	97 (164)	129 (219)	129 (219)	129 (219)
Fly Ash (kg/m^3, lb/yd^3)	-	-	-	-	-	-	-	-
Silica fume (kg/m^3, lb/yd^3)	33 (55)	33 (55)	33 (55)	33 (55)	33 (55)	-	-	-
Total cementitious material (kg/m^3, lb/yd^3)	648 (1095)	648 (1095)	648 (1095)	648 (1095)	648 (1095)	648 (1095)	648 (1095)	648 (1095)
W/C ratio	0.4	0.4	0.4	0.4	0.4	0.4	0.4	0.4
Fine aggregate/Sand (kg/m3, lb/yd3)	1296 (2190)	1296 (2190)	1296 (2190)	1296 (2190)	1296 (2190)	1296 (2190)	1296 (2190)	1296 (2190)
HRWR (kg/m3, oz./yd3)	2 (54)	4 (108)	4 (108)	4 (108)	2 (54)	2 (54)	2 (54)	2 (54)
Shrinkage Reducing Admixture (gal./yd^3)	1	1	1	1	1	1	1	1
Macro Fiber (PPF) vol% & Length (in)	-	0.1% 0.75 in.	-	-	-	-	0.1% 0.75 in.	-
Micro Fibers (PPF) vol% & Length (in)	-	-	0.1% 1.5 in.	-	-	-	-	-
Steel Fibers (STF) vol% & Length (in)	-	-	-	0.1% 2.0 in.	0.1% 0.75 in.	-	-	0.1% 0.75 in.
C4 and C5: Group four control mixes PPF: Macro Synthetic Fiber (PPF) STF: Steel Fiber								

High Performance Concrete

The concrete mix design proposed for investigating FRP tendons was tested and mixed in Rutgers Laboratory. The mix proportions are summarized in Table 2.10 and as shown the mix includes silica fume. The addition of such materials was utilized to create high performance concrete mix that achieves all the limits specified in the standards. The mix achieved around 12 ksi compressive strength in 28 days that corresponded to 5454 psi modulus of elasticity. The selection of the mix design was mainly based on the 28 days compressive strength as well as the workability of the mix.

Class A Concrete

The mix design for the Class A concrete was implemented as a standard mix in many of the NJ bridges and structures. The mix design is summarized in Table 2.11 below. This mix is utilized in casting the damaged beams that are repaired with the FR-SCC and FR-FC mortars.

Table 2.10. HPC Mixture Proportions

Mixture Proportions	HPC Mix
Type I Portland (kg/m^3, lb/yd^3)	661 (1120)
Silica fume (kg/m^3, lb/yd^3)	67 (112)
Total cementitious material (kg/m^3, lb/yd^3)	728 (1232)
W/C ratio	0.28
Fine aggregate/Sand, (kg/m^3, lb/yd^3)	554 (924)
Coarse aggregate (kg/m^3, lb/yd^3)	1033 (1722)
HRWR (kg/m^3, oz./yd^3)	4 (108)

Table 2.11. Class A Mixture Proportions

Mixture Proportions	Class A
Type I Portland (kg/m^3, lb/yd^3)	390 (658)
Total cementitious (kg/m^3, lb/yd^3)	390 (658)
W/C ratio	0.41
Coarse aggregate (kg/m^3, lb/yd^3)	1065 (1800)
Fine aggregate/Sand (kg/m^3, lb/yd^3)	714 (1205)
HRWR (kg/m^3, oz./yd^3)	4 (108)
AEA (kg/m^3, oz./yd^3)	1 (27)

2.3. Mixing Procedure

2.3.1. Fiber Reinforced Ferrocement (FR-FC)

Mortar mixes were performed according to ASTM standards C305 using the equipment's presented in Figure 2.1. As described in specification C511, the room temperature and the humidity and the water temperature were maintained to be 23.0 +/- 4.0°C. Mixing water was first introduced in the bowl, followed by the cement, mixed for 30 seconds, and then the sand was added gradually while mixing at a slow speed. Speed increased for 45 seconds long and then fibers were introduced to the paste for another 30 seconds. Mixing paused, mortar stuck on the side of the bowl was scraped down. Finish by mixing for a minute at a medium speed.

The mixing sequence for the FR-FC mixtures consisted of homogenizing the sand for 60 sec, before introducing half of the mixing water. The cementitious materials were then added and mixed for 30 sec followed by the Fibers followed by the HRWR diluted in the remaining water. The mortar was mixed for 4 min and remained at rest for 2 min for any adjustments.

Figure 2.1. Mortar Mixer

2.3.2. Concrete Mixtures

Prior to every mix, the appropriate amount of batching material is pre-batched into several clean buckets, labeled, and organized as to increase productivity of the mixing process itself. Moisture content is performed three hours before every mix and adjustments are made as needed to prevent modifications for the water/cement ratio.

Following ASTM C192, the mixing procedure for the concrete mixtures that were prepared using a drum mixer with 6 ft^3 capacity is as follows:

1) Homogenize sand and coarse aggregate for 30 sec.
2) Incorporate coarse aggregate, half of the mixing water, and AEA into the mixer and mix for 1 min.
3) Add the powder materials and mix for 30 sec.
4) Add half of the remaining water, and mix for 1 min.
5) Add the remaining water and HRWR, fibers, and mix for 3 min (and SRA if used).
6) Keep the concrete at rest for 3 min followed by remixing for additional 3 min.

2.4. Test Methods

2.4.1. Test Methods for Mortar Mixtures

Mortar mixtures were made to evaluate the performance of different SCM types and replacement rates on fresh and hardened properties as well as to assess the effect of various fibers dosages and types on drying shrinkage, and compressive strength development. The laboratory investigations used for concrete equivalent mortar (no coarse aggregate) are presented below.

Drying shrinkage

Drying shrinkage of the mortar (ASTM C596) was determined using a digital length comparator to measure changes in length of prismatic specimens measuring 25 × 25 × 285 mm (1 × 1 × 11.25 in.). After demolding at 24h, the prisms were immersed in water for the curing period needed (3, 7, 14 days), then the samples were transferred to a temperature and humidity controlled room set at 23 ± 1 °C (74 ± 2 °F) and 50 ± 3% RH, and the shrinkage was monitored until the age of 56 days.

Compressive strength

The 1-, 3-, 7-, 28-, and 56-day compressive strengths of mortars were determined using 50-mm cube specimens according to ASTM C109. The cubes were demolded after one day and stored in lime-saturated water at 21 ± 2 °C (70 ± 4 °F) until testing age. The results of compressive strength represent the average values of four specimens.

2.4.2. Test Methods for Concrete Mixtures

Fresh Concrete Properties for Fiber Reinforced Self-Consolidating Concrete (FR-SCC)

The team measured the concrete fresh properties for the SCC mixes in accordance with ASTM C1611 which uses the inverted slump cone to measure slump flow. The time elapsed between lifting of the slump cone and slump flow reaching a 20 in. diameter was measured as the T20 time in seconds. When the flow stopped, the largest diameter as well as a 90^{o} offset of that diameter were recorded and averaged for the slump flow.

The segregation and bleeding were observed after the slump flow test and before cleaning the base plate. A VSI of 0 (zero) indicates no bleeding or segregation, and a VSI of 1 means slightly visible bleeding in the form of sheen on the concrete. When a slight mortar halo appears around the edges of the slump flow less than 12.7 mm (1/2 in.) in thickness, the concrete is deemed unstable with a VSI of 2. If the halo exceeds 12.7 mm (1/2 in.) in thickness or a pile of aggregate is visibly segregated in the center of the slump flow, a VSI of 3 is assigned and the concrete is deemed highly unstable. Only VSI less than 1 is acceptable for application. Moreover, the J-ring test was performed in accordance with ASTM C1621 to determine passing ability. A 12 in. diameter of metal J-Ring with 16 vertical rebars was used for this test. The slump cone was filled and lifted as it was in the slump flow test, so that the SCC flowed through the vertical rebars. When the concrete stopped flowing, the largest diameter and 90-degree offset diameter from the largest were measured and averaged to calculate the J-ring flow. In general, the J-ring value is compared to the slump flow to determine the blocking assessment. A difference of less than 1 in. indicates no significant blocking of the flow. When the difference is between 25.4 and 50.8 mm (1 and 2 in.), minimal blocking may be occurring. The difference of greater than 50.8 mm (2 in.) indicates extreme blocking.

In addition to the ASTM standards, the team also performed the L-box test as a comparative measure of passing ability (Raymond, 2012). The L-box consists of a 600 mm (24 in.) high, 100 × 200 mm (4 × 8 in.) shaft with a hole measuring 150 × 200 mm (6× 8 in.) at the bottom. The gate covering the hole leads to a tray measuring 600 mm (24 in.) long and 200 mm (8 in.) wide onto which the concrete flows. The concrete was scooped into the top of the shaft and allowed to fall to the bottom while the gate was closed. Once the shaft was filled, the concrete sat for one minute and then leveled without the use of any compaction or vibration. The gate was then lifted so that the concrete was allowed to pass through three 9.5 mm (3/8 in.) diameter steel rebar at 25 mm (1 in.) spacing and onto the tray. After the flow stopped, the concrete height was taken at the wall of the gate opening (h1) and at the opposite end of the tray (h2). The ratio of these two heights (h1/h2) was taken and compared between mixtures to see the performance of each mixture in a confined space.

A Type B pressure air meter was used to determine the air content of the concrete mixtures according to ASTM C231. The pressure air test was performed immediately after the slump flow test. The unit weight, yield and gravimetric air content were measured using the procedure dictated by ASTM C138. The test used the same measuring bowl used for the pressure air content to calculate concrete density and the air content by means of the gravimetric air content test. The difference in the theoretical density of the components and the actual density of the concrete, is due to the entrainment of air within the concrete.

Mechanical Property Test

Compressive strength tests were performed at 28 days after casting according to ASTM C39. The cylinders were capped with a sulfur capping compound in accordance with ASTM C617 to ensure a flat surface for consistent results. Three cylinders were used and the average values were determined to represent the strength at 28 days. If the compressive strength varied more than 10% from other results, the result was discarded and an additional cylinder was tested.

Splitting tensile strength and modulus of elasticity were measured for each mixture at 28 days in accordance with ASTM C496 and C469, respectively. For tensile strength, each specimen was placed horizontally in the testing machine between two 1 in. wide pieces of plywood. The cylinder was then loaded until splitting occurred. Three specimens were tested for each mixture to ensure accuracy, and 10% variance rule was also applied. For modulus of elasticity, samples were also capped with sulfur, similar to the compression test. The cylinders were loaded until 35–40% of their compressive strength with displacement readings being taken every 1814 kg (4,000 lb). Each cylinder was tested twice for consistency and three specimens were tested for each mixture.

Free Shrinkage Test

Free shrinkage measurements were taken regularly using a length comparator according to ASTM C157. Two prism samples 75 × 75 × 300 mm (3 in. wide × 3 in. deep × 11-3/4 in. long) per mixture were prepared with two embedded stainless-steel studs at both ends. Samples were stored and tested in an environmentally controlled environment at 24 ºC (74 ºF) and 50% relative humidity to prevent any thermal expansion. At each testing period, a reference bar was placed into the length comparator and the minimum length reading was taken. The prism sample was then placed into the length comparator and the minimum measurement was recorded. The process was repeated for each sample at least twice per week over the course of testing period of 28 days.

3. CONCRETE PERFORMANCE EVALUATION

3.1. Fresh Properties

3.1.1. Test Methods for Concrete Mixtures

The slump flow test was performed in accordance with ASTM C1611 using the inverted slump cone. Slump flow was the first test performed after the concrete batch was mixed properly. The target slump flow was between 550 mm (21.5) in. and 650 mm (25.5 in.). the same dosage of HRWR were added to all the other subsequent mixes as the control mixtures to compensate the reduction of slump flow due to the addition of fibers. Table 3.1 shows the slump flows after HRWR adjustment. The results clearly show that a reduction in the concrete flow was observed and the mixtures with PPF fibers obtained lower than the minimum required slump flow of 432 mm (17 in.) with as little as 0.30% fiber by volume. It is important to determine the passing ability of an SCC mixture for field implementation in which the concrete should pass smoothly through tightly spaced reinforcement. As the J-ring value is highly dependent on the flowability, the mixture is considered to have an adequate passing ability if the J-ring test result is within 75 mm (3 in.) of the total slump flow. The J-ring values are presented in Table 3.1. It was noticed that mixtures containing fibers up to 0.3% vol could pass the J-ring requirement set forth herein. However, once fiber volume increased further, passing ability became a big concern, and PPF3 0.30 mixtures obtained the flow loss of 102 mm (4 in.) in the presence of tightly packed reinforcement.

Table 3.1. Slump Flow Values and J-Ring Test Results

Slump Results	PPF 0.00	PPF1 0.30	PPF1 0.50	PPF2 0.30	PPF3 0.30	STF2 0.20	STF2 0.50	HPPF1 0.11	HSTF2 0.16
HRWR (kg/m3, fl. oz./yd^3)	2.5 (68)	3 (81)	3 (81)	3.5 (95)	3.5 (95)	3.5 (95)	3 (81)	3.5 (95)	3.5 (95)
Slump flow (mm, in.)	559 (22)	546 (21.5)	483 (19.0)	508 (20.0)	559 (22.0)	546 (21.5)	559 (22.0)	521 (20.5)	546 (21.5)
J-ring (mm, in.)	521 (20.5)	495 (19.5)	445 (17.5)	432 (17.0)	457 (18.0)	508 (20.0)	521 (20.5)	470 (18.5)	495 (19.5)
+/- Slump (mm, in.)	-38 (-1.5)	-51 (-2.0)	-38 (-1.5)	-76 (-3.0)	-102 (-4.0)	-38 (-1.5)	-38 (-1.5)	-51 (-2.0)	-51 (-2.0)

3.1.2. T20 and Visual Stability Index (VSI)

The T20 time was measured simultaneously with the slump flow test. The T20 time was limited within 20 seconds in order to assure the flowability of the SCC within a relatively short period of time. As a low-viscosity SCC mixture is generally preferred, the team designed the mix to obtain a minimum 2 seconds of T20 time for the control mixture. Table 3.2 summarizes the T20 test results. The results show that the viscosity and T20 time generally increased with higher fiber content. While the total slump flow remained relatively close for each mixture, the flow moved slower for the higher fiber mixtures. The VSI was taken immediately after the slump flow was measured. Table 3.2 presents the VSI results of four mixtures tested in this study. The first two mixtures (control mixture and minimum fiber mixture) obtained the same VSI of 0 indicating unlikely to segregate or bleed. As fibers were added and slump flow was inhibited slightly, a halo-like ring was formed around the slump flow indicating segregation may have occurred. For PPF2 0.3 and HPPF 0.11 mixtures, the halo-like rings remained small but the aggregate did not visibly segregate after the slump flow test, therefore it was determined to have a VSI of 1. While a VSI of 1 was the highest found in the mixtures in this study, trial mixtures have shown that additional fibers could lead to a higher degree of segregation (VSI of 2 or 3). The VSI of 0 is considered ideal, and the VSI of 1 also is acceptable in most cases. The VSI of 2 or 3 indicates the mixture is not ready for field implementation and additional measures must be taken to reduce segregation which was not the case here for any of the mixes.

Table 3.2. T20 and VSI Test Results

Mixture	PPF 0.00	PPF1 0.30	PPF1 0.50	PPF2 0.30	PPF3 0.30	STF2 0.20	STF2 0.50	HPPF1 0.11	HSTF2 0.16
T20 (s)	4.5	3.94	8.58	6.67	6.4	4.43	5.25	6	5.1
VSI	0	0	0	1	0	0	0	1	0

3.1.3. Air Content

Proper air content is a necessity to achieve to give the concrete the chance to breath where freeze and thaw cycles is a concern. The targeted air content of 4-8% by volume is recommended, and Table 3.3 shows the air contents measured. In general, the air content increases as the fiber content increases; however, this is deemed to be a side-effect of the increased dosage of HRWR with higher fiber volume.

Table 3.3. Air Content Test Results

Mixture	PPF 0.00	PPF1 0.30	PPF1 0.50	PPF2 0.30	PPF3 0.3	STF2 0.2	STF2 0.5	HPPF1 0.11	HSTF2 0.16
Air Content (%)	6.5	6.2	6.6	6.8	6.8	6.2	7.0	6.4	6.4

3.2. Mechanical Properties

3.2.1. Fiber Reinforced Self-Consolidating Concrete (FR-SCC)

Mechanical properties including compression, tension, and modulus of elasticity were tested for the FR-SCC mixtures at 28 days after mixing. The samples were stored in the environmental chamber to provide steady temperature of 24°C (74°F) and RH of 50%. A total of 9 cylindrical samples from each mixture were used for the mechanical testing. Six samples were sulfur capped to distribute the stress uniformly on the cylinder during the compression and modulus of elasticity testing (three cylinders each). The remaining 3 samples were used for the splitting tensile strength test. The cracking strain which is the splitting tensile strength divided by the modulus of elasticity, was calculated and this value represents the maximum strain this mix can sustain before any cracking occurs.

Table 3.4 summarizes the testing results of these mixtures. The parentheses next to each value indicate the percentage difference compared to control mixture, PPF 0.00.

Table 3.4. Mechanical Properties (% difference compared to the control mix, PPF 0.00)

	PPF 0.00	PPF1 0.30	PPF1 0.50	PPF2 0.30	PPF3 0.3	STF2 0.2	STF2 0.5	HPPF1 0.11	HSTF2 0.16
Compressive strength (MPa, psi)	41.7 (6051)	32 (4618) (-23%)	35 (5076) (-16%)	34.3 (4976) (-18%)	38.4 (5573) (-8%)	39 (5653) (-6%)	37.3 (5414) (-11%)	46.4 (6728) (11%)	42 (6091) (1%)
Tensile Strength (MPa, psi)	2.83 (410)	2.62 (380) (-7%)	2.95 (428) (4%)	3.39 (492) (20%)	3.39 (492) (20%)	3.2 (466) (14%)	3.2 (468) (14%)	3.63 (527) (29%)	3.7 (537) (31%)
Elastic Modulus (GPa, ksi)	24.8 (3604)	24.9 (3611) (0.4%)	23.2 (3364) (-7%)	24.6 (3565) (-1%)	24.4 (3535) (-2%)	25.7 (3730) (4%)	26 (3777) (5%)	27.4 (3979) (10%)	26.5 (3840) (7%)
Cracking Strain (με)	113	105 (-7%)	127 (12%)	138 (22%)	139 (23%)	125 (11%)	123 (9%)	132 (17%)	140 (24%)

It was noticed that the fiber content slightly decreases the compressive strength of the mixture. The reduction reached up to 23% with 0.3% of PPF fibers. This is because the strength of the concrete comes from the bond between cement paste and aggregate, and the flexible fibers mixed added to the cement matrix may weaken the bond strength. The splitting tensile strength, however, increased with the addition of fibers up to 31%. The friction between cement paste and the fibers improved the tensile strength which helped prevent pulling out and made the concrete more ductile. The increase in tensile strength and decrease in modulus of elasticity resulted in higher cracking strain and is a key to increase the cracking resistance which mitigates cracking shown in the restrained shrinkage rings.

3.2.2. Fiber Reinforced Ferrocement (FR-FC)

The best 14 FR-FC mixes were promoted for next phase. Mechanical properties including compression and tension were tested at 28 days after mixing. The samples were stored in the environmental chamber to provide steady temperature of 24^{o}C (74^{o}F) and RH of 50%. The base ferro-cement mixture is summaries in Table 3.5 and the variables of the best 14 FR-FC mixes are summarized in Table 3.6.

Table 3.5. Mix Design for Base Mortar Mix

Mixture ID	Control Mix
Type I Portland cement (kg/m3, lb/yd3)	650 (1095)
Total cementitious material (kg/m3, lb/yd3)	650 (1095)
Fine aggregate/Sand (kg/m3, lb/yd3)	1296 (2190)
Water (kg/m3, lb/yd3)	260 (438)
HRWR (kg/m3, oz./yd3)	4 (108)
Shrinkage Reducing Admixture (gal./yd3)	4.95 (1)

Table 3.6. Fiber Content of Each Mortar Mix Group

Group	Cementitious Material	Mix ID	Description/ Variables
Group 1	Cement Only	C1 (control mix)	No fiber
		C1PPF	0.1% vol. Macro PPF (0.75 in or 19 mm)
		C1STF	0.1% vol. STF (0.75 in or 19 mm)
Group 2	5% Silica Fume	C2 (control mix)	No fiber
		C2PPF	0.2% vol. Macro PPF (0.75 in or 19 mm)
		C2STF	0.1% vol. STF (0.75 in or 19 mm)
		C2PPF1	0.1% vol. Macro PPF (0.75 in or 19 mm)
		C2PPF2	0.1% vol. Macro PPF (1 in or 25 mm)
		C2PPF3	0.1% vol. Macro PPF (1.5 in or 38 mm)
		C2H1	0.1% vol. Macro PPF (1 in or 25 mm) + 0.1% vol. Macro PPF (0.75 in or 19 mm)
		C2H2	0.1% vol. Macro PPF (1 in or 25 mm) + 0.1% vol. STF (0.75 in or 19 mm)
Group 3	5% Silica Fume + 20% Fly Ash	C3 (control mix)	No fiber
		C3PPF	0.1% vol. Macro PPF (0.75 in or 19 mm)
		C3STF	0.1% vol. STF (0.75 in or 19 mm)

Table 3.7 summarizes the testing results of these mixtures. The parentheses next to each value indicate the percentage difference compared to control mixture for each group. Incorporating fly ash and silica fume shows an improvement on compressive strength with the addition of PPF fibers by 23.7% and 14.4% when STF fibers are added. For tensile strength, the mixes with hybrid fibers provide the most improvements (C2H1 and C2H2) by 23 and 32% compared to their control mix.

Table 3.7. Mechanical Properties of FR-FC

Group	Cementitious Material	Mix ID	Compressive Strength (psi, MPa)	Tensile Strength (psi, MPa)
Group 1	Cement Only	C1 (control mix)	47.4 (6875)	3.2 (467)
		C1PPF	56.2 (8150) (18.6%)	2.9 (425) (-8%)
		C1STF	56.2 (8150) (18.6%)	3.85 (559) (+20)
Group 2	5% Silica Fume	C2 (control mix)	49.6 (7200)	3.4 (495)
		C2PPF	51.3 (7450) (3.5%)	2.4 (353) (-28%)
		C2STF	50.3 (7302) (1.42%)	4.2 (610) (+23%)
		C2PPF1	51.4 (7450) (3.5%)	3.4 (495) (0%)
		C2PPF2	48.7 (7063) (-1.9%)	3.1 (442) (-10%)
		C2PPF3	51.5 (7475) (3.8%)	4.1 (599) (+21%)
		C2H1	52.5 (7612) (5.7%)	4.2 (611) (+23%)
		C2H2	54.1 (7855) (9.1%)	4.5 (654) (+32%)
Group 3	5% Silica Fume + 20% Fly Ash	C3 (control mix)	44.3 (6425)	2.9 (421)
		C3PPF	54.8 (7950) (24%)	3.6 (527) (+25%)
		C3STF	50.7 (7350) (14%)	3.1 (450) (+7%)

3.3. Free Shrinkage properties

3.3.1. Fiber Reinforced Self-Consolidating Concrete (FR-SCC)

Comparator measurements for free shrinkage were taken throughout the testing period at least twice every week. Figure 3.1 and Table 3.8 represents the free shrinkage results of this study. It was observed that free shrinkage decreased as fiber content increased. When PPF fibers were added at 0.30% by volume, free shrinkage decreased by 15%. However, the shrinkage improvement was not as effective as other studies. It was reported that the free shrinkage of fiber-reinforced concrete was about two-thirds of the control mixture when the fiber content was up to 0.75% by volume (Saje, 2011). Such small improvement of free shrinkage strain in this study could be a result of the curing regime, because it was reported that the absence of curing increased the ultimate free shrinkage as well as the shrinkage rate (Na, 2013). The fact that the shrinkage specimens without moisture curing after 1 day may greatly influence the free shrinkage while the effect of fibers was negligible compared with curing regime.

Table 3.8. Shrinkage Properties

Shrinkage	PPF 0.00	PPF1 0.30	PPF1 0.50	PPF2 0.30	PPF3 0.3	STF2 0.2	STF2 0.5	HPPF1 0.11	HSTF2 0.16
7 days of curing (με)	505	427	527	545	525	370	525	355	455
% Change from dry curing	-29%	-35%	-45%	-19%	-39%	-34%	-48%	-39%	-26%
% change from control mix	-	-15%	+4%	+8%	+4%	-27%	+4%	-30%	-12%

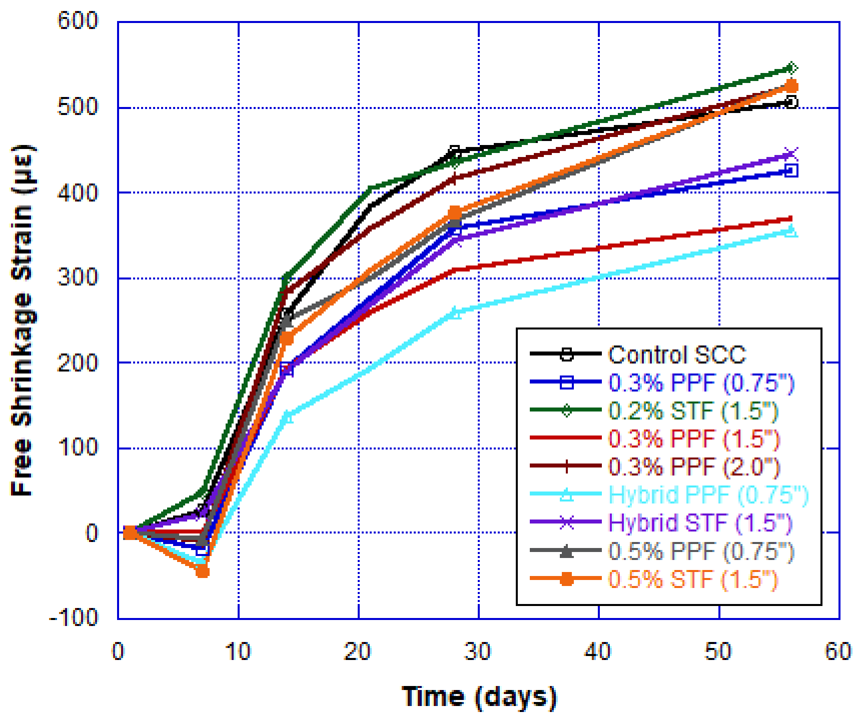

Figure 3.1. Free Shrinkage Strain (μs) vs Time (Days) for FR-SCC Mixes

3.3.2. Fiber Reinforced Ferrocement (FR-FC)

Comparator measurements for free shrinkage were taken throughout the testing period at least twice every week. Table 3.9 represents the free shrinkage results of this study. It was observed that free shrinkage decreased when fibers are included for most mixes. The highest improvements were notices with the two hybrid mixes C2H1 and C2H2 by 21 and 24%, respectively.

Table 3.9. Free Shrinkage Strain of FR-FC

Group	Cementitious Material	Mix ID	Free Shrinkage Strain (με)
Group 1	Cement Only	C1 (control mix)	695
		C1PPF	740 (+6%)
		C1STF	746 (+7%)
Group 2	5% Silica Fume	C2 (control mix)	520
		C2PPF	620 (+19%)
		C2STF	463 (-10%)
		C2PPF1	491 (-5%)
		C2PPF2	430 (-18%)
		C2PPF3	475 (-8%)
		C2H1	410 (-21%)
		C2H2	395 (-24%)
Group 3	5% Silica Fume + 20% Fly Ash	C3 (control mix)	561
		C3PPF	440 (-22%)
		C3STF	413 (-26%)

4. BEAM TESTING DETAILS AND RESULTS

The aim of this section is to validate the performance of FR-SCC and FR-FC in small-scale elements. Large-scale specimens were casted to validate the performance of the CFRP tendons which is described in detail below.

4.1. Structural Performance of Concrete Beams Repaired with FR-SCC and FR-FC

4.1.1. Specimens Preparation

Small-scale beams were prepared for this study to evaluate the effect of FR-FC and FR-SCC combined with different steel reinforcements in the laminate of composite retrofitted beams. These beams were tested in four-point bending. For this investigation, the shear reinforcement size and type, rebar in the laminate, and number of mesh layer provided in the laminate were varied. Shear reinforcements are also referred to as shear studs due to their effect on composite action for this application. While substrate reinforcement remained consistent throughout this experiment, stud size and arrangement were varied. Figure 4.1 provides a section view of two stud arrangements. The stud arrangement varied for beams without any steel reinforcement in the laminate to provide enough shear strength to guarantee a flexural failure, as seen in Figure 4.1. Five different FC and SCC mixes and utilized for these beams repair testing.

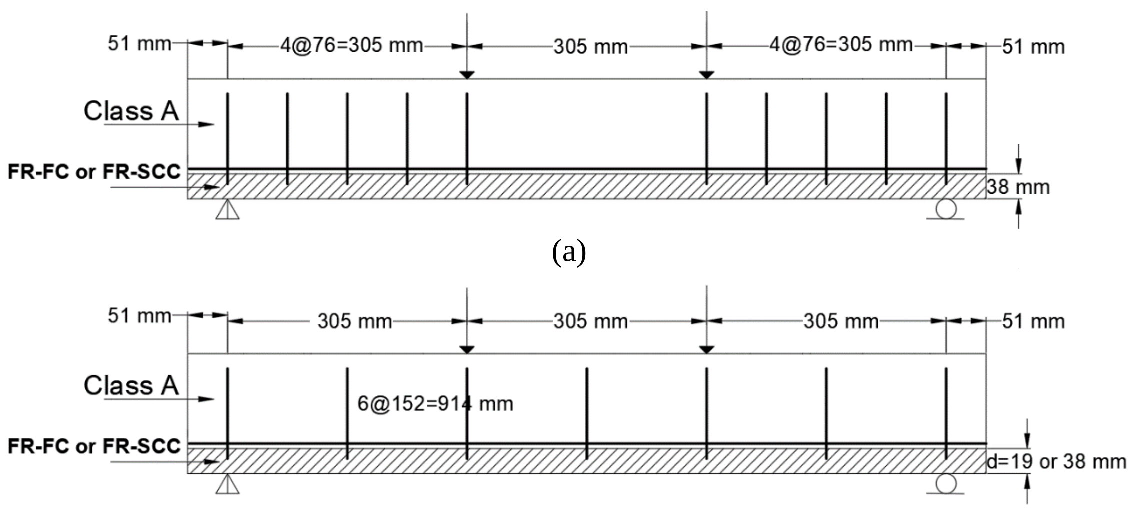

(b)

Figure 4.1. Specimen Dimensions; (a) Beam Set Number 1 & 2 and (b) Beam Set Number 3 & 4

Retrofitted beams were casted in two phases. The first phase was casting of the substrate concrete. For the substrate, Class A concrete was used. Four beams were casted monolithically with Class A as control beams. Class A was mixed and casted into the beams then consolidated using mechanical vibration. For beams which were subsequently to be casted with laminates, a line was drawn on the inside of the wooden formwork to ensure the proper thickness of substrate was. Once casted, wet burlap was placed on the fresh concrete and the beams were sealed in plastic sheet to prevent moisture from escaping. All beams were cured using wet burlap and rewet daily. Samples which were taken from batches used to cast beams substrate or laminate were cured in the same manner of the beams. These samples remained next to the beams throughout the entire testing cycle, even after the wet curing period was finished. Laminates were casted after the substrate layers are properly cured. Prior to the laminate casting, all extra exposed steel and loose concrete was cleaned and removed. This included removing the steel ties which held the stirrups in place and using a hammer and chisel to remove concrete which may have hardened on the stirrups. This was done to ensure a clean steel surface, allowing for the best bond between the substrate and laminate. For beams containing mesh, the mesh was tied to the stirrups to prevent them from moving during concrete placement as presented in Figure 4.2

Figure 4.2. Install Laminates Prior to Casting Repair Material

All beams were tested in four-point bending with supports and point loads applied as shown in Figure 4.3. A Test Resources machine was used to apply load, as this machine has a moving base which controlled the loading rate. Beams were tested at a constant loading rate of 900 pounds per minute, in accordance with ASTM C78 for the beams respective dimensions. Beams were place on two rollers offset 2” from the edge of the beam, with two point-loads being applied at 12” from each support. Crack mapping was also performed during testing once first cracks appeared. At any appearance of a new crack, the load that initiated the crack was recorded. Pictures of the cracks were cracks were taken during the tests at approximately 500-pound increments.

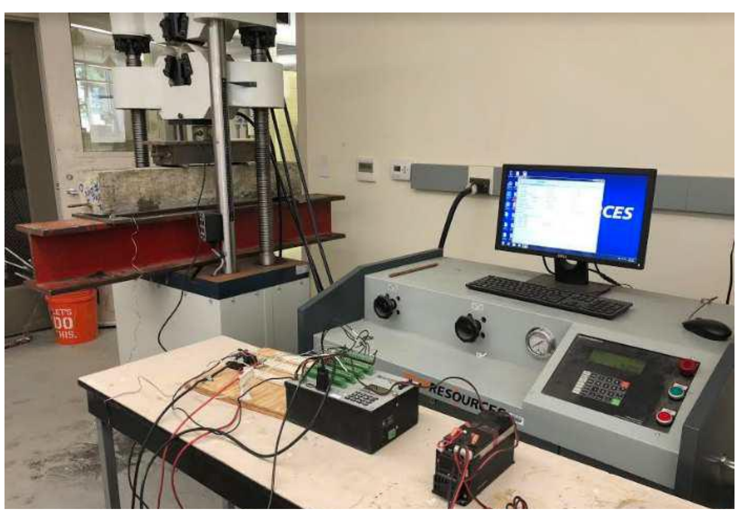

Figure 4.3. Small Beam Testing Setup

A total of 44 beams were tested in four-point bending. Beams were either casted monolithically with Class A concrete, or retrofitted using FR-SCC or FR-RC laminates, with certain retrofitted beams contain mesh reinforcement and rebar in the laminates to provide additional load carrying capacity. Load, deflection, strain data and cracking measurements were collected for each specimen tested.

Based on the hardened properties, four FR-SCC and FR-FC mixes were selected to be used for the laminate. Table 4.1 and Table 4.2 presents the detailed testing program for each repair material.

Nomenclature for the Beam IDs mentioned in Table 4.1 and Table 4.2 provide information of the beam characteristics, and are as shown as Aa-B-C-y%, where:

- "A" represents the layer type
- "a" represents the beam set number (1, 2, 3 or 4 as shown in Figure 4.1)
- "B" represents the number of mesh layer.
- "C" represents the shear stud bar size (2 is #6 and 3 is #10)
- "y%" represents fiber dosage for the repair layers or mix designation label

Table 4.1. FR-SCC Testing Program

Aa-B-C-y%	Mix Designation	Concrete cover (mm/inch)	f'c (Mpa/ksi)	# of Layers	Studs Size
SCC1-5-3-H1	HPPF1-0.11	25/1	28.3/4	5	#10
SCC1-0-3-0	PPF-0.00	38/1.5	33.1/4.8	-	#10
SCC1-0-3-0	PPF-0.00	38/1.5	33.1/4.8	-	#10
SCC1-8-2-H1	HPPF1-0.11	38/1.5	28.3/4	8	#6
SCC1-5-2-H1	HPPF1-0.11	25/1	28.3/4	5	#6
CB-2	Class A	-	-	-	#6
SCC2-0-3-H2	HSTF2-0.16	38/1.5	29/4.2	-	#10
SCC2-0-3-H2	HSTF2-0.16	38/1.5	29/4.2	-	#10
SCC2-0-3- P2	PPF1-0.5	38/1.5	31.7/4.6	-	#10
SCC2-0-3- P2	PPF1-0.5	38/1.5	31.7/4.6	-	#10
SCC2-0-3-P1	PPF1-0.30	38/1.5	24.1/3.5	-	#10
SCC2-0-3-P1	PPF1-0.30	38/1.5	24.1/3.5	-	#10
CB-4	Class A	-	-	-	#10
SCC3-8-3-0	PPF-0.00	38/1.5	37.9/5.5	8	#10
SCC3-5-3-0	PPF-0.00	38/1.5	37.9/5.5	5	#10
SCC3-8-3-H2	HSTF2-0.16	38/1.5	33.1/4.8	8	#10
SCC3-5-3-H2	HSTF2-0.16	38/1.5	33.1/4.8	5	#10
SCC3-8-3-P2	PPF1-0.5	38/1.5	42.7/6	8	#10
SCC3-5-3-P2	PPF1-0.5	38/1.5	42.7/6	5	#10
SCC4-0-3-H1	HPPF1-0.11	38/1.5	37.2/5.4	-	#10
SCC4-8-3-H1	HPPF1-0.11	38/1.5	37.2/5.4	8	#10
SCC4-5-3-H1	HPPF1-0.11	38/1.5	37.2/5.4	5	#10

Table 4.2. FR-FC Testing Program

Aa-B-C-y%	Mix Designation	Concrete cover (mm)	f'c (MPa/ksi)	# of Layers	Studs Size
CB-1	Class A	-	-	-	#10
FC1-8-3-0.1	C3PPF	38/1.5	51.7/7.5	8	#10
FC1-8-3-0.0	C3	38/1.5	51.7/7.5	8	#10
FC1-5-3-0.1	C3PPF	25/1	51.7/7.5	5	#10
FC1-5-2-0.2	C2PPF	25/1	51.7/7.5	5	#6
FC1-8-2-0.1	C3PPF	38/1.5	51.7/7.5	8	#6
FC2-0-3-0	C3	38/1.5	51.7/7.5	-	#10
FC2-0-3-0	C3	38/1.5	51.7/7.5	-	#10
FC2-0-3-0.2	C2PPF	38/1.5	51.7/7.5	-	#10
FC2-0-3-0.2	C2PPF	38/1.5	51.7/7.5	-	#10
FC2-4-3-0.2	C2PPF	38/1.5	51.7/7.5	4	#10
FC2-4-3-0.2	C2PPF	38/1.5	51.7/7.5	4	#10
CB-3	Class A	-	-	-	#10
FC2-5-3-0.2	C2PPF	38/1.5	51.7/7.5	5	#10
FC2-8-3-0.2	C2PPF	38/1.5	51.7/7.5	8	#10
FC1-8-3-0.1	C3PPF	38/1.5	51.7/7.5	8	#10
FC2-0-3-H1	C2H1	38/1.5	51.7/7.5	-	#10
FC2-5-3-H1	C2H1	38/1.5	51.7/7.5	5	#10
FC2-8-3-H1	C2H1	38/1.5	51.7/7.5	8	#10
FC2-0-3-H2	C2H2	38/1.5	51.7/7.5	-	#10
FC2-5-3-H2	C2H2	38/1.5	51.7/7.5	5	#10
FC2-8-3-H2	C2H2	38/1.5	51.7	8	#10

4.1.2. Results of FR-SCC and FR-FC Reinforced Concrete Beams

The cracking load (Pcr), the cracking deflection (δcr), the ultimate load (Pu) and the corresponding ultimate deflection (δu) for all the tested beams have been determined. The test results of all specimens will be discussed in this section with respect to their strength, load-deflection response curves, and failure modes. The obtained experimental results for all the tested specimens are summarized in Table 4.3 and Table 4.4.

Compared to the control beam, all tested specimens strengthened with FR-SCC layer showed an improved performance in terms of cracking load and ultimate load as presented in Table 4.3 and Figure 4.4. The increase in the cracking load ranged from a 22% up to 228% and for the ultimate load ranged from 41.5% to 62% for the layers where fibers are incorporated. In addition, it was observed that the improvement in the cracking load was minor with no improvement in the ultimate load or the deflection, when the fibers are missing and the beams are strengthened with the control SCC mix. The incorporation of fiber in the SCC mix enhanced the cracking resistance for all specimens, ranging from 31% up to 53% compared to the control beam. The influence of FR-SCC laminates with no steel mesh or reinforcement has a negative effect on the ultimate capacity and the deflection.

Table 4.3. FR-SCC Testing Results

Beam ID	Cracking Load, Pcr (kN/kips)	Ultimate Load, Pu (kN/kips)	Deflection @ Ultimate Load, Δu (mm/in)
CB-2	14.2/3.2	41.8/9.4	15.5/0.61
SCC1-0-3-0	18.2/4 (+28.1%)	31.6/7 (-24.5%)	15.0/0.59 (-3.1%)
SCC1-0-3-0	17.3/ 3.9 (+21.9%)	36.9/8.3 (-11.7%)	14.7/0.57 (-5.1%)
SCC1-8-2- H1	44.5/10 (+212.5%)	67.6/15.2 (+61.7%)	8.9/0.35 (-42.5%)
SCC1-5-2- H1	41.4/9.3 (+190.6%)	60.9/13.7 (+45.7%)	7.1/0.28 (-54.4%)
SCC1-5-3-H1	46.7/10.5 (+228.1%)	59.2/13 (+41.5%)	6.8/0.27 (-56.1%)
SCC2-0-3-H2	18.7/4.2 (+31.3%)	33.4/7.5 (-20.2%)	20.1/0.8 (29.7%)
SCC2-0-3-H2	19.1/4.3 (+34.4%)	32.9/7.4 (-21.3%)	-
SCC2-0-3-P2	21.8/5 (+53.1%)	37.4/8.4 (-10.6%)	19.3/0.7 (+24.3%)
SCC2-0-3-P2	19.6/4.4 (+37.5%)	37.8/8.5 (-9.6%)	17.6/ (+13.6%)
SCC2-0-3-0.3	18.7/4.2 (+31.3%)	31.1/7 (-25.5%)	13.8/0.54 (-11.1%)
SCC2-0-3-0.3	19.6/4.4 (+37.5%)	39.6/9 (-5.3%)	15.7/0.62 (+1.1%)
CB-4	18.7/4.2	49.4/11.1	13.8/0.54
SCC3-8-3-0	44.9/10.1 (+140.5%)	80.5/18.1 (+63.1%)	4.8/0.19 (-65.3%)
SCC3-5-3-0	41.8/9.4 (+123.8%)	66.7/15 (+35.1%)	5.0/0.19 (-64.0%)
SCC3-8-3-H2	63.2/14.2 (+238.1%)	85.9/19.3 (+73.9%)	5.2/0.2 (-62.6%)
SCC3-5-3-H2	36.0/8.1 (+92.9%)	57.8/13 (+17.1%)	4.9/0.19 (-64.8%)
SCC3-8-3- P2	40.5/9.1 (+116.7%)	89.0/20 (+80.2%)	4.9/0.19 (-64.8%)
SCC3-5-3- P2	37.8/8.5 (+102.4%)	66.3/15 (+34.2%)	5.1/0.2 (-63.3%)
SCC4-0-3-H1	20.5/4.6 (+9.5%)	31.6/7 (-36%)	14.6/0.57 (+5.7%)
SCC4-8-3-H1	44.0/9.9 (+135.7%)	65.8/14.8 (+33.3%)	4.6/0.18 (-66.6%)
SCC4-5-3-H1	39.1/8.8 (+109.5%)	58.7/13.2 (+18.9%)	5.1/0.2 (-63.3%)

Table 4.4. FR-FC Testing Results

Beam ID	Cracking Load, Pcr (kN/kips)	Ultimate Load, Pu (kN/kips)	Deflection @ Ultimate Load, Δu (mm/in)
CB-1	16.9/ 3.8	37.8/8.5	10.8/0.43
FC1-8-3-0.1	34.3/7.7 (+102.6%)	56.6/12.7 (+49.4%)	5.5/0.22 (-49.2%)
FC1-8-3-0.0	22.7/5.1 (+34.2%)	42.7/9.6 (+12.9%)	4.6/0.18 (-57.6%)
FC1-5-3-0.1	45.4/10.2 (+168.4%)	68.5/14.7 (+81.2%)	5.0/0.2(-54.1%)
FC1-5-2-0.2	37.4/8.4 (+121.1%)	58.3/13.1 (+54.1%)	4.6/0.18(-57.4%)
FC1-8-2-0.1	35.6/8 (+110.5%)	78.7/17.7 (+108.2%)	6.1/0.24(-43.8%)
FC2-0-3-0.0	16.9/3.8 (0%)	29.8/6.7 (-21.2%)	12.2/0.48 (+12.2%)
FC2-0-3-0.0	18.7/4.2 (+10.5%)	33.8/7.6 (-10.6%)	14.2/0.56 (+31.4%)
FC2-0-3-0.2	18.2/4 (+7.9%)	36/8 (-4.7%)	13.9/0.55 (+28.6%)
FC2-0-3-0.2	19.6/4.4 (+15.8%)	32.9/7.4 (-12.9%)	15.8/0.62 (+45.5%)
FC2-4-3-0.2	38.7/8.7 (+128.9%)	58.7/13.2 (+55.3%)	5.0/0.2 (-53.9%)
FC2-4-3-0.2	42.3/9.5 (+150%)	59.6/13.4 (+57.6%)	4.6/0.18 (-57.4%)
CB-2	26.2/5.9	41.8/9.4	15.2/0.6
FC3-5-3-0.2	30.2/6.8 (+15.3%)	71.2/16 (+70.2%)	5.4/0.21 (-64.8%)
FC3-8-3-0.2	37.8/8.5 (+44.1%)	86.3/19.4 (+106.4%)	2.9/0.11 (-80.7%)
FC3-8-3-0.1	32.5/7.3 (+23.7%)	54.7/12.3 (+30.9%)	3.5/0.14 (-77.3%)
FC3-0-3-H1	21.8/4.9 (-16.9%)	37.8/8.5 (-9.6%)	13.2/0.52 (-13.2%)
FC3-5-3-H1	37.8/8.5 (+44.1%)	65.4/14.7 (+56.4%)	4.5/0.18 (-70.7%)
FC3-8-3-H1	48.9/11 (+86.4%)	88.5/19.8 (+111.7%)	5.6/0.22 (-63.6%)
FC3-0-3-H2	20.0/4.5 (-23.7%)	38.7/8.7 (-7.4%)	14.7/0.58 (-3.3%)
FC3-5-3-H2	36.0/8.1 (+37.3%)	66.3/14.9 (+58.5%)	5.2/0.2 (-65.8%)
FC3-8-3-H2	35.1/7.9 (+33.9%)	74.4/16.8 (+78.7%)	4.4/0.17 (-71.2%)

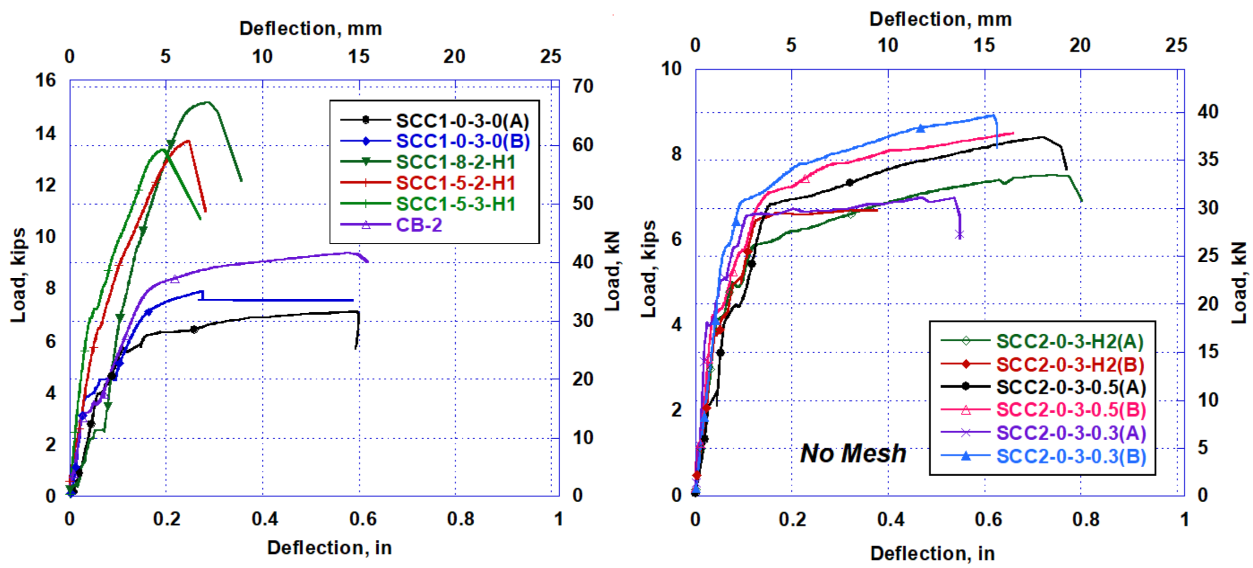

Figure 4.4. Load-Deflection Response for FR-SCC Beams, (a) Compared to Control Beams and (b) Effect of Fibers Only

Figure 4.5 shows the effect of each FR-SCC mix on the beam performance at 0, 3, and 8 layers of mesh. The highest ultimate load was achieved by P2 (0.5% PPF fibers) FR-SCC mix with 8 layers of mesh. However, the cracking load was improved the most by H1 mix (combining PPF with STF).

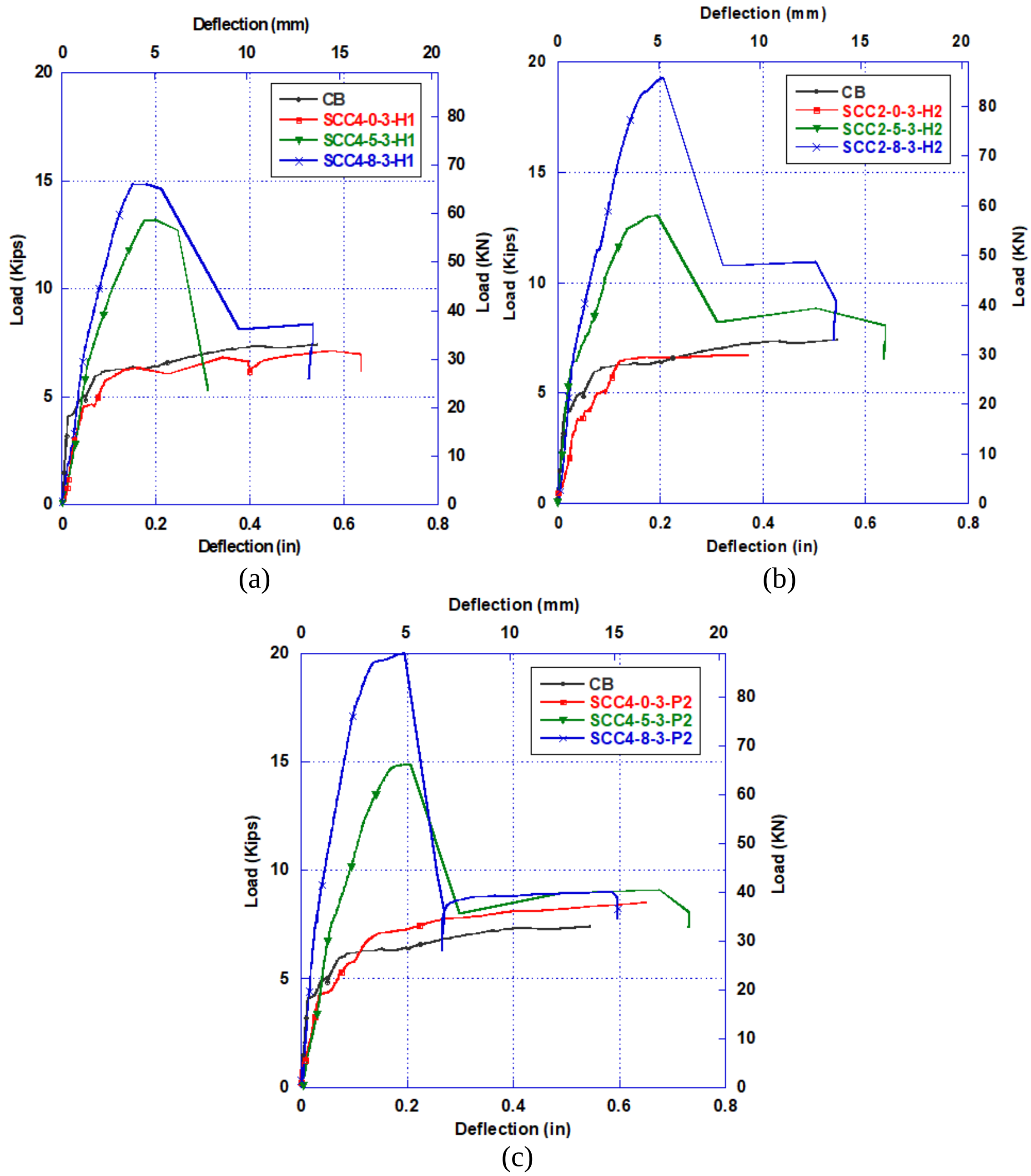

Figure 4.5. Load-Deflection Response, (a) H1 Mixes, (b) H2 Mixes, (c) P2 Mixes

Using only PPF fibers with 0.5% in the SCC laminate improved the cracking load and achieved the highest ultimate capacity for the same number of meshes. This effect was observed with 5 and 8 meshes as sown in Figure 4.6.

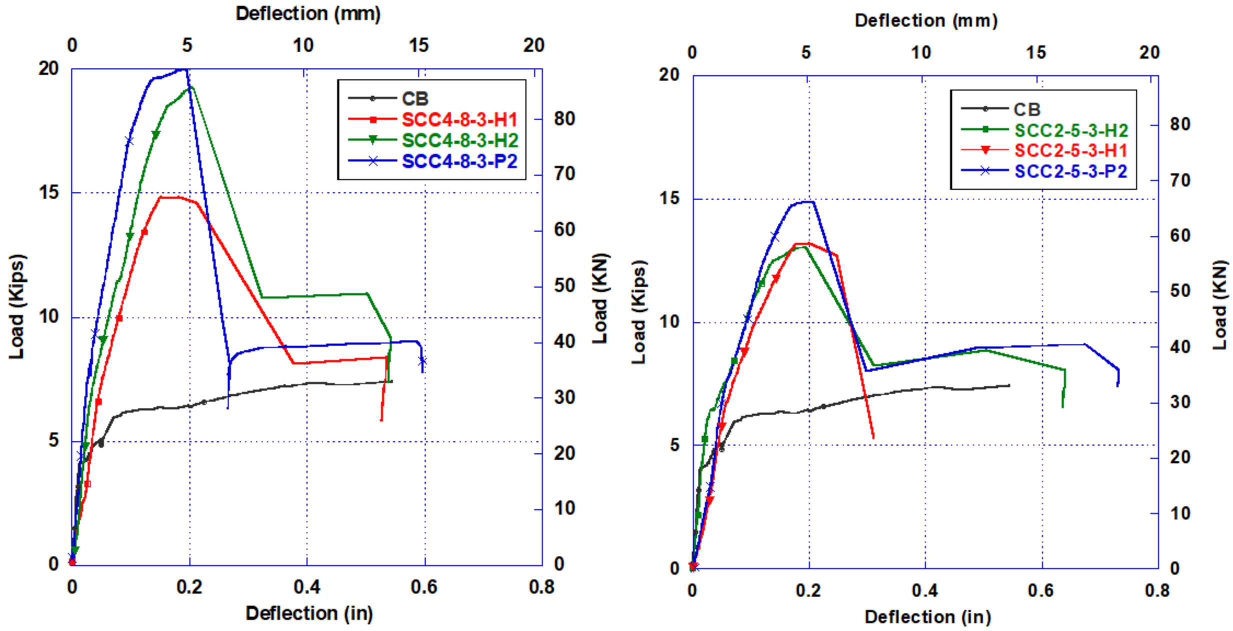

Figure 4.6. Load-Deflection Response, (a) 8 Layers, (b) 5 Layers

Table 4.5 and Figure 4.7 present the cracking performance of the specimens repaired with FR-SCC. The results show that the use of fibers has a direct effect on the number of cracks and the maximum crack with of each specimen.

Table 4.5. FR-SCC Cracking Performance Results

Beam ID	# of Cracks	Max Crack Width (mm/in)
CB-4	3	2.93/0.11
SCC3-8-3-0	7 (+133%)	0.15/0.006 (-85%)
SCC3-5-3-0	6 (+100%)	0.301/0.012 (-70%)
SCC3-8-3-H2	2 (-33.3%)	0.16/0.006 (-84%)
SCC3-5-3-H2	5 (+66.6%)	0.38/0.014 (-62%)
SCC3-8-3-0.5	7 (+133.3%)	0.38/0.014 (-62%)
SCC3-5-3-0.5	5 (+66.6%)	0.34/0.013 (-66.7%)
SCC4-0-3-H1	4 (+33.3%)	0.23/0.009 (-77%)
SCC4-8-3-H1	5 (+66.7%)	0.15/0.0059 (-85%)
SCC4-5-3-H1	6 (+100%)	0.1/0.00393 (-90%)

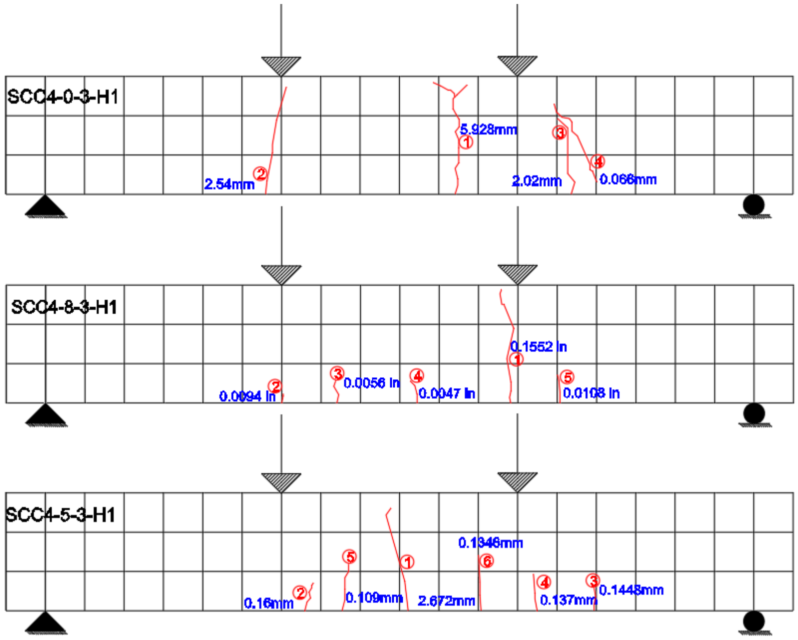

Figure 4.7. Cracking Performance of FR-SCC Specimens (SCC)

Compared to the control beam, all beams strengthened with FR-FC layer improved in terms of cracking load and ultimate load as presented in Figure 4.8 and Table 4.4 The cracking load improved from 34% to 168% and the ultimate load improved from 14% to 109%. However, the deflection was reduced from 43.8% up to 57.6% compared to the control beam. In addition, Beams with mesh had 114% increase in cracking load and 71% increase in ultimate load compared to beams with No mesh and fibers. Also, Beams with mesh had 128% increase in cracking load and 87% increase in ultimate load compared to beams with no mesh and no fibers. The testing results shows that 0.2% fiber addition without mesh had small increase in cracking and ultimate load 6% and 9% respectively.

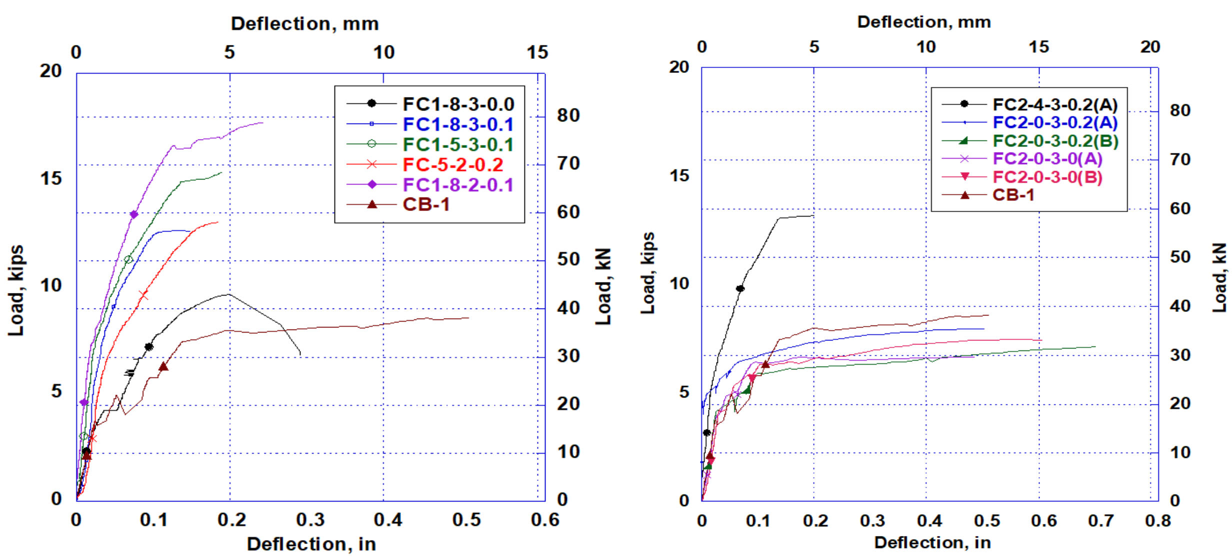

(a) (b)

Figure 4.8. Load-Deflection Response for FR-FC Beams, (a) Compared to Control Beams and (b) Effect of Fibers Only

Figure 4.9 shows that combining micro PPF fibers with STF (H1) in the FR-FC laminate improved the cracking load and achieved the highest ultimate capacity for the same number of meshes.

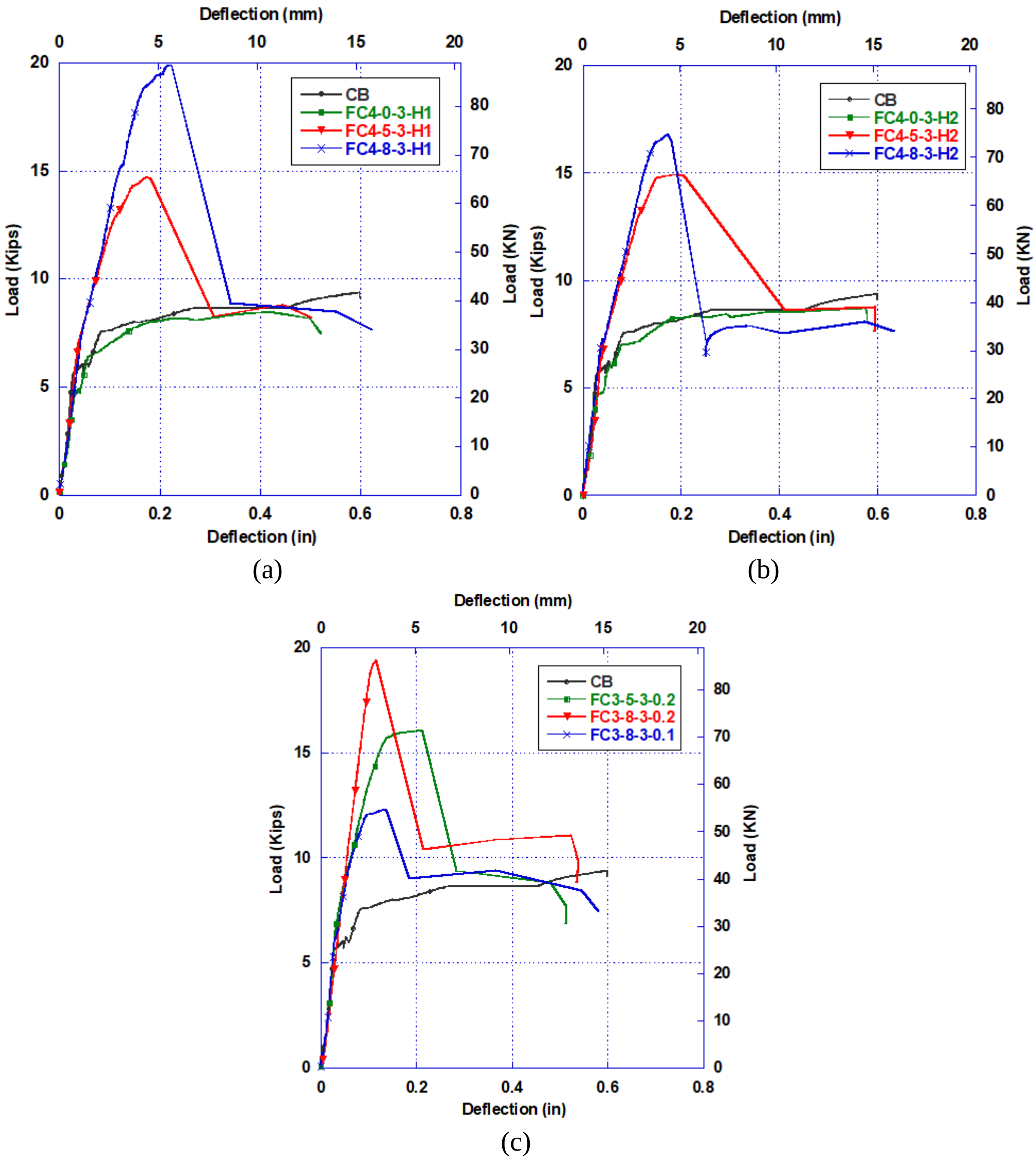

Figure 4.9. Load-Deflection Response, (a) H1 Mix, (b) H2 Mix, (c) 0.1 & 0.2% Fiber Mix

The fibers content has minor effect on the ultimate capacity of the beams. The increase achieved was maximum 12% when fibers content increase from 0.1 to 0.2% of PPF fibers as shown in Figure 4.10. The cracking load is highly increase by the increase of the fibers concrete or the use of hybrid fibers in the same mix (STF + PPF).

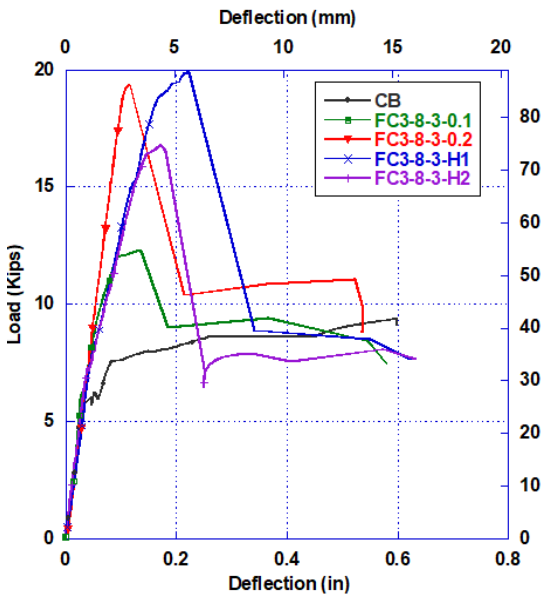

(a)

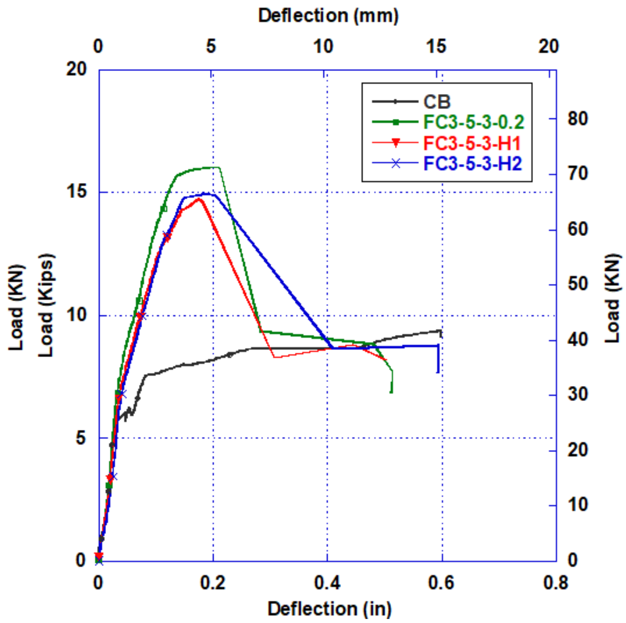

(b)

Figure 4.10. Load-Deflection Response, (a) 8 Layers, (b) 5 Layers

Table 4.6 and Figure 4.11 present the cracking performance of the specimens repaired with FR-FC. The results show that the use of fibers has a direct effect on the number of cracks and the maximum crack with of each specimen. H1 Mix (steel fibers with micro PPF fibers) improved the number of cracks and crack width by 266.7% and -63.3%. The use of the fibers has a direct effect on the max crack width at ultimate

Table 4.6. FR-FC Cracking Performance Results

Beam ID	# of Cracks	Max Crack Width (mm/in)
CB-3	3	3.23/0.13
FC2-5-3-0.2	6 (+100%)	0.11/0.004 (-64.8%)
FC2-8-3-0.2	9 (+200%)	0.12/0.0047 (-80.1%)
FC1-8-3-0.1	3 (+0%)	0.37/0.014 (-77.3%)
FC3-0-3-H1	4 (+33%)	1.90/0.075 (-13.1%)
FC3-5-3-H1	7 (+133%)	0.29/0.011 (-70.7%)
FC3-8-3-H1	11 (+267%)	0.39/0.015 (-63.3%)
FC4-0-3-H2	3 (+0%)	1.89/0.074 (-3.33%)
FC4-5-3-H2	9 (+200%)	0.19/0.0075 (-65.8%)
FC4-8-3-H2	9 (+200%)	0.254/0.01 (-71.2%)

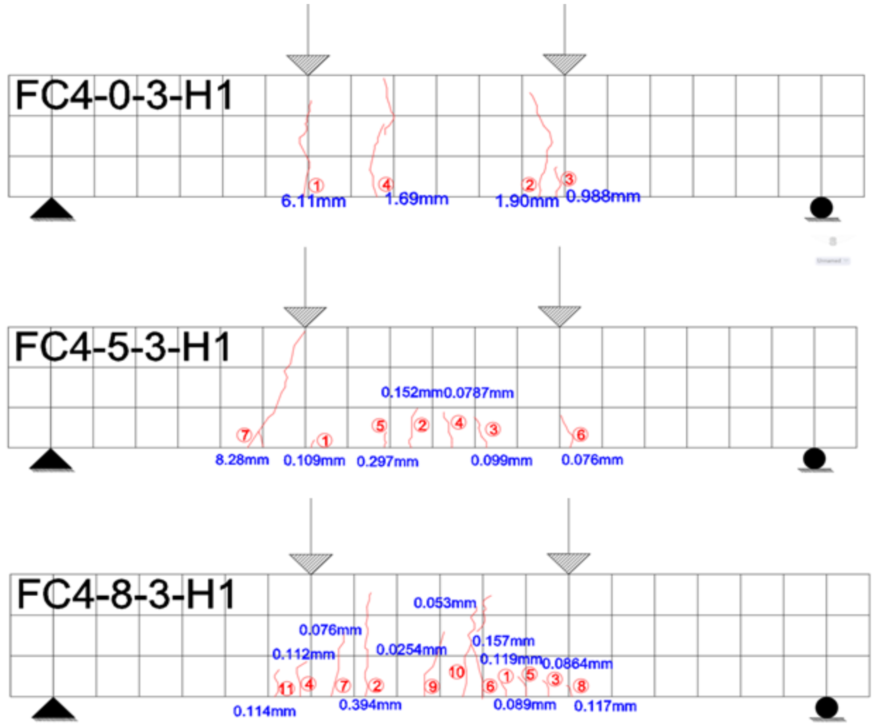

Figure 4.11. Cracking Performance of FR-FC Specimens (FC)

4.1.3. Comparison of FR-SCC and FR-FC Reinforced Concrete Beams

The test program presented strengthening RC beams with FR-SCC and FR-FC mixes and the results, presented in Figure 4.12 and Table 4.7, are reported and a comparison between both techniques are summarized below:

1) The cracking load has improved up to 238% for the FR-SCC beams and up to 63% for the FR-FC beams.

2) The difference in the improvement in ultimate load among beams repaired with FR-SCC and FR-FC are similar especially when the same fibers are introduced to the mix

3) Both techniques increase the number of crack prior to failure up to 200% for the FR-FC beams and 133% for the FR-SCC beams. The number of crack is an important indication of the ductility improvements of the retrofitted beams.

4) Crack widths have been improved by both techniques dramatically which is so important to delay the chloride penetration to the concrete reinforcement. The crack width has improved between 3 to 80% for the FR-FC and 62 to 90% for the FR-SCC beams.

Table 4.7. FR-FC vs FR-SCC Cracking Performance Results

Beam ID	Cracking Load, P_{cr} (kN/kips)	Ultimate Load, P_u (kN/kips)	Deflection @ Ultimate Load, Δ_u (mm/in)
FC3-5-3-0.2	30.2/6.8	71.2/16	5.4/0.212
SCC3-5-3-P2	37.8/8.5	66.3/14.9	5.1/0.2
FC4-8-3-0.2	37.8/8.5	86.3/19.4	2.9/0.11
SCC4-8-3-P2	40.5/9.1	89.0/20	4.9/0.19
FC3-5-3-H2	36.0/8.1	66.3/14.9	5.2/0.2
SCC3-5-3-H2	36.0/8.1	57.8/13	4.9/0.19
FC4-8-3-H2	35.1/7.9	74.7/16.8	4.4/0.173
SCC4-8-3-H2	63.2/14.2	85.9/19.3	5.2/0.20

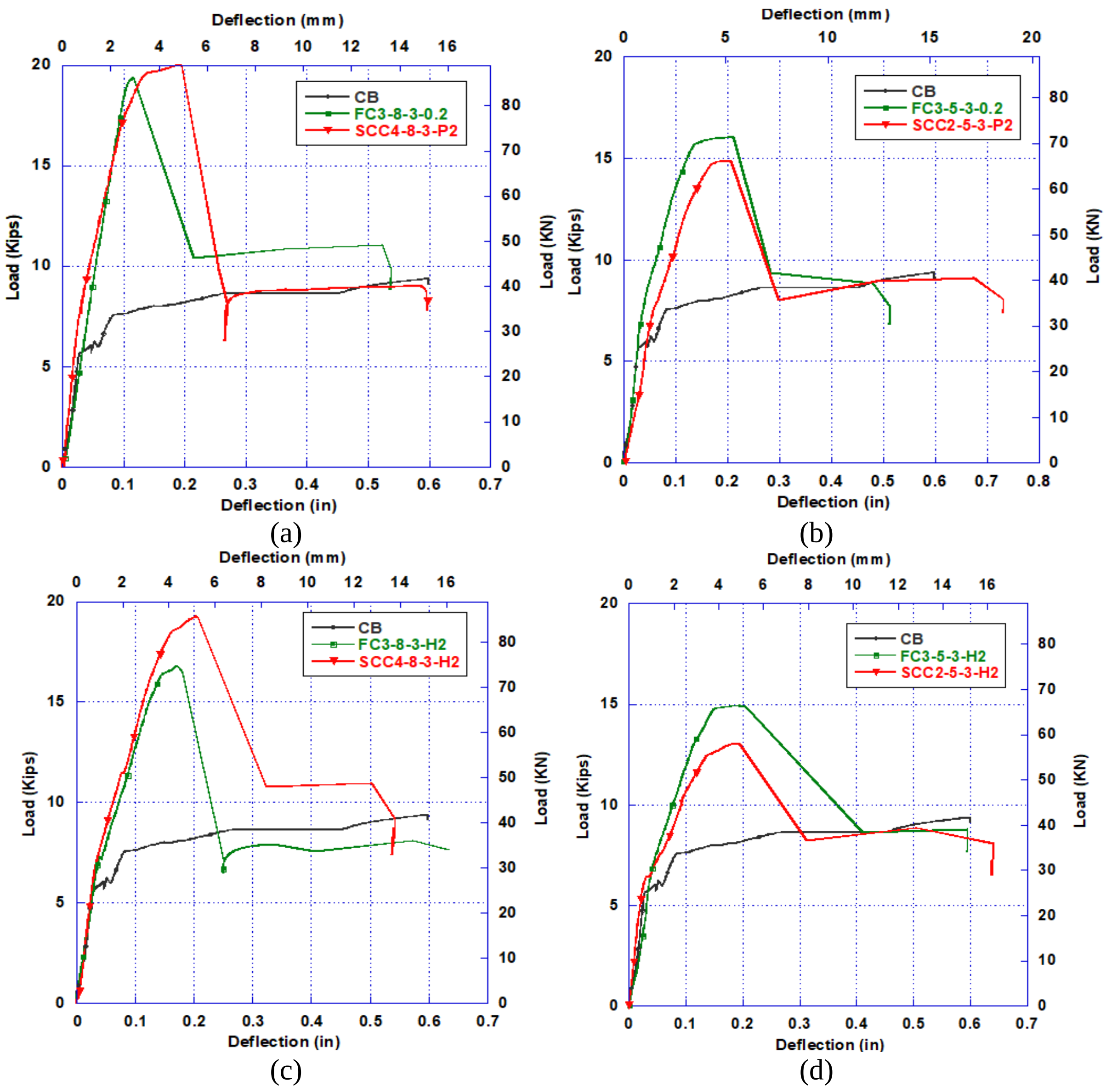

Figure 4.12. Load-Deflection Response for FR-SCC vs FR-FC

4.2. Structural Performance of Prestressed Concrete Beams with Hybrid Tendons

4.2.1. Specimens Preparation

A total of 15 beams was casted and tested in Rutgers laboratory. The different parameters that was considered in this program are

- The area of the unbonded tendons, A_{ups}
- The area of the bonded tendons, A_{bps}
- The unbonded tendons material (CFRP or Steel)
- Depth of unbonded and bonded tendons
- Span Length, L

All prestressed beams were simply supported with straight tendon profile and tested with third point loading. Below is a flowchart of the various tasks that were needed to accomplish the experimental program to be completed. Each task presented in the chart will be expanded on each in details. As shown in the chart below (Figure 4.13) the experimental work will go through four phases which are materials and setup preparation, casting the large-scale beams, post-tensioning and testing the beams and finally data analysis.

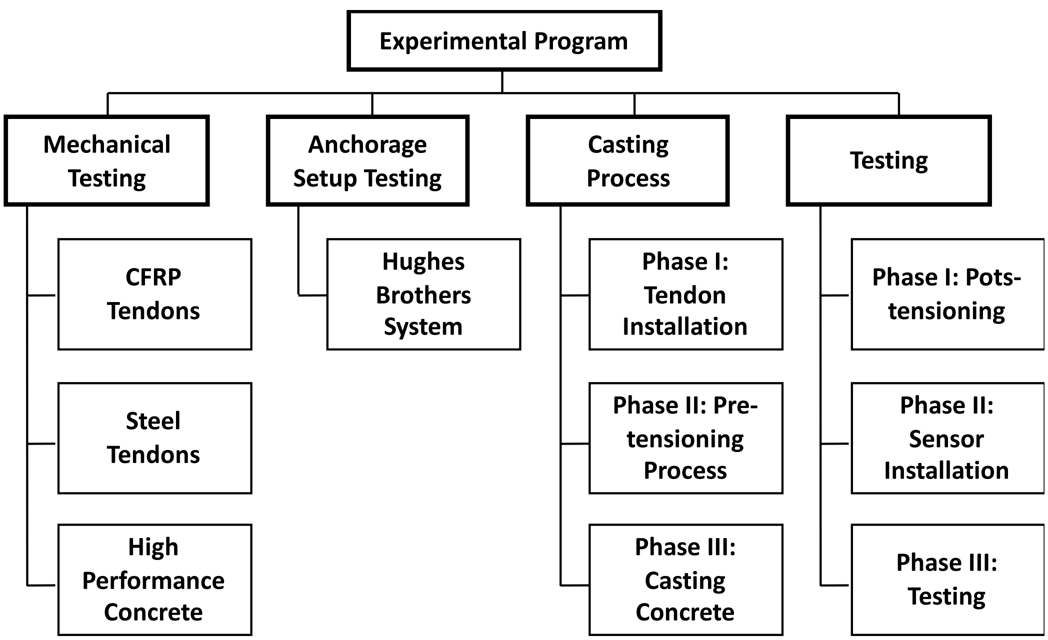

Figure 4.13. Experimental Program Plan Chart

Aslan 250 CFRP tendon was used to post-tension the reinforced and pretensioned concrete beams. These tendons were purchased from Hughes brother's company that has variety of bars and tendons that have been used in many studies and researches. To develop the full tensile capacity of the tendons, each one has a steel anchorage that can be affixed on both sides. The anchorage is used as a grip to clamp the tendons on the dead end while prestressing and also to transfer the jacking force for the steel rebar connected to the CFRP tendon, as shown in Figure 4.14. Aslan 250 tendons have many benefits when compared to steel tendons such as they won't corrode and impervious to chloride ion and chemical attacks. Also, the weight to strength ratio of the CFRP tendons is higher than the steel strands. The handling and placement of such tendons are similar to steel but with the benefit of weighing one-fifth the weight of steel. The CFRP tendons that was used in this study have a nominal area of 0.11 and 0.196 in^2. The tendons ultimate stresses are 350 and 340 ksi, the ultimate strain is 1.75 and 1.67% and the modulus of elasticity are 18000 ksi, respectively for #3 and #4 tendons. The tendons mechanical properties are summarized in Table 4.8.

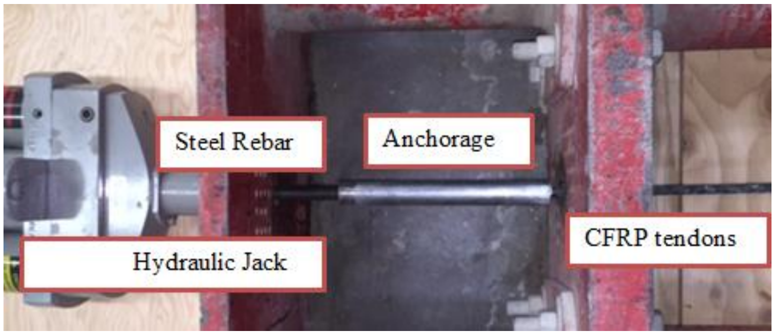

Figure 4.14. Steel Anchorage Jacking using Aslan 250 Tendons

Table 4.8 Mechanical Properties of CFRP Tendons (Hughes Brothers)

Size	Diameter	Area	f_{fu}	Ultimate Tensile Load	E_f	Ultimate strain
#3	9.5 mm 3/8 in	71 mm^2 0.11 in^2	315 ksi 2172 MPa	34.7 kips 154 kN	18x106 psi 12x104 MPa	1.75%
#4	12.7 mm 1/2 in	126 mm^2 0.196 in^2	300 ksi 2068 MPa	58.8 kips 262 kN	18 x106 psi 12x104 MPa	1.67%

Figure 4.15 illustrates a typical cross-section and elevation of beams proposed for the testing program. The dimensions are: h=10 in, hf=2.25 in, b=12 in, and bw=5 in. Table 4.9 summarizes the parameters for all proposed 15 specimens and below describes the notation of each beam (A-L-C).

- A: Prestressed System – U for unbonded tendon, B for bonded, H for hybrid
- L: Bottom Tendon Properties, XYZ: X for Area (in^2), Y for B or U, Z for Tendon Material (F for CFRP and S for Steel)
- C: Top Tendon Properties, XYZ: X for Area (in^2), Y for B or U, Z for Tendon Material (F for CFRP and S for Steel)

Table 4.9. Summary of Beam Properties and Parameters (f'c= 12 ksi, ds = 9 in, As = 0.22 in^2)

Group	Un-bonded Tendon	No.	Designation	Bottom Tendon		Top Tendon		.)
				A_{ps} (in^2/mm^2)	d_{bp} (in/mm)	A_{ps} (in^2/mm^2)	d_{up} (in/mm)	
Control beams	-	1	BB-0.085	0.085/55	8.8/233	0.085/55	7.5/190.5	120
	Steel	2	UU-0.085	0.085/55	8.8/233	0.085/55	7.5/190.5	120
Unbonded Beams	Steel	3	U-0.085S	-	-	0.085/55	6.125/155	120
		4	U-0.153S	-	-	0.153/99	6.125/155	120
	CFRP	5	U-0.11F	-	-	0.11/71	6.125/155	96
		6	U-0.11F	-	-	0.11/71	6.125/155	120
		7	U-0.19F	-	-	0.19/123	6.125/155	120
Hybrid Beams	Steel	8	H-0.085US-0.085BS-D	0.085/55	7.5/190.5	0.085/55	8.8/233	120
		9	H-0.085BS-0.085US	0.085/55	8.8/233	0.085/55	6.125/155	120
		10	H-0.085BS-0.153US	0.085/55	8.8/233	0.153/99	6.125/155	120
		11	H-0.153BS-0.153US	0.153/99	8.8/233	0.153/99	6.125/155	120
	CFRP	12	H-0.11UF - 0.085BS-D	0.085/55	7.5/190.5	0.11/71	8.8/233	120
		13	H-0.085BS-0.11UF	0.085/55	8.8/233	0.11/71	6.125/155	120
		14	H-0.085BS-0.19UF	0.085/55	8.8/233	0.19/123	6.125/155	120
		15	H-0.153BS-0.11UF	0.153/99	8.8/233	0.11/71	6.125/155	120

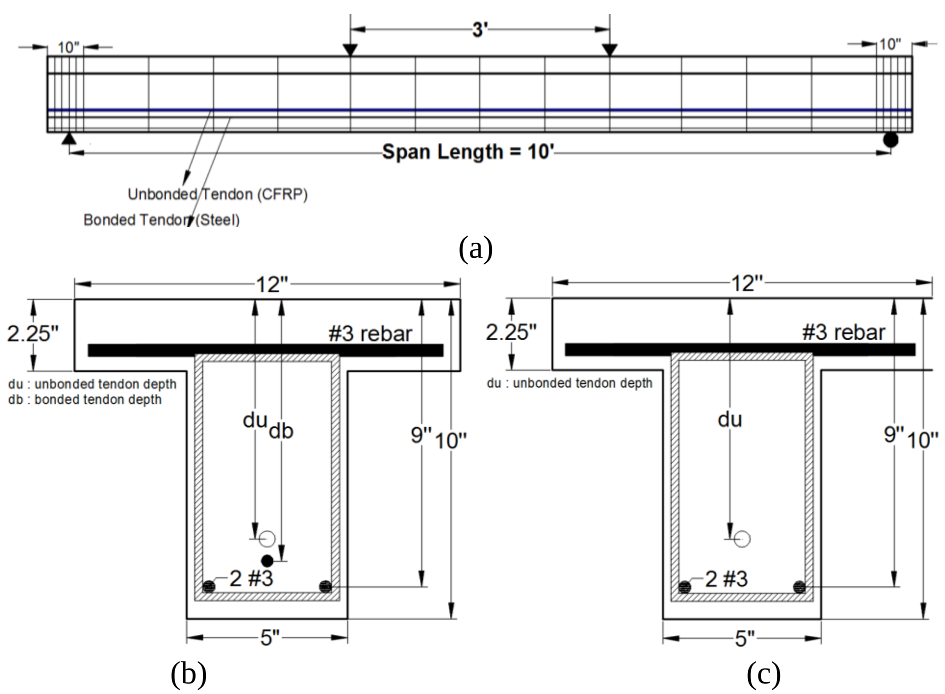

Figure 4.15. Beam Design and Cross Section Details; (a) Beam Design, (b) Hybrid Beam Cross Section, and (c) Unbonded Beam Cross Section

The testing will take place the same day of post-tensioning which will be around the 28 days age of concrete. In that age, the concrete compressive strength is expected to be around 12 ksi and the cracking strain is around 161 $\mu\varepsilon$. All beams were tested under four points loading until failure and each specimen will have foil strain gauges, LVDTs and load cells installed in several locations on the beams to measure the strain, deflections and the ultimate stress in both concrete and the strands.

Also, schematic diagram of the locations of the LVDTs, strain gauges, and load cells, on the tested beams are shown in Figure 4.16. In addition to the schematic diagram in Figure 4.16, Table 4.10 summarizes each sensor and the purpose of using it.

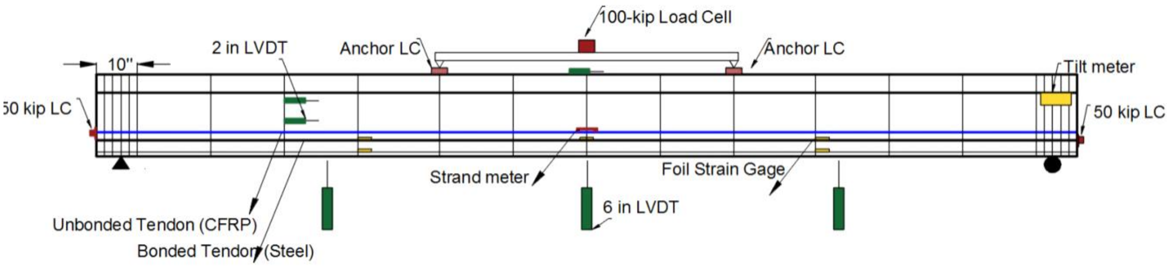

Figure 4.16. Overview of Loading Frame and Strain Measuring Instruments Locations

Table 4.10. Overview of Each Sensors Details and Purpose

Sensor	Detail	Reason
Linear Variable Differential Transformer (LVDT)		Two types of LVDTs supplied by RDP were used, which had 6.0 in and 2.0 in range capacities. LVDTs will measure the beam Deflection in several locations and to measure the Strain at beam extreme fiber.
Load Cell (50 kips)		The 50-kip capacity load cells were used to monitor the force in the prestressing strand while jacking and testing (f_{pe}, f_{ps}).
Load Cell (100 kip)		The 100-kip load cell were attached to the hydraulic actuator of the closed-loop testing frame and will be used to monitor the externally applied load on beam during testing (P).
Foil Strain Gage	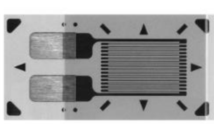	Foil strain gages were attached on the flexure Reinforcing Bars and the Prestressing Strands (CFRP and steel). Two to Three strain gages were placed on each rebar/ strand.

4.2.2. Hybrid Beams Testing Results

The deflections at several locations of the specimen were recorded during the testing of the member until failure. The camber was measured on the frame for beams that are post-tensioned with steel tendons. However, the camber for the beams post-tensioned with CFRP tendons are measured during the tensioning on the lab reaction floor. The deflection values for the tested specimens are all summarized in Table 4.11. The mid-span deflection is recorded for each beam at the cracking of concrete, yielding of the non-prestressed steel, yielding of the bonded tendons, yielding of the unbonded tendons and at concrete crushing at top. The load-deflection curves given in Figure 4.17 through Figure 4.23 are presented in groups that shows the effects of the Aps (bonded), Aps (unbonded), the unbonded tendons materials and depth on the load-deflection performance. The increase in the bonded strand area achieved an increase in the load ultimate carrying capacity up to 88% in H-0.153BS-0.11UF, which corresponded to an increase in the deflection up to 33% compared to U-0.11 that did not include any prestressed bonded tendons. Although the use of CFRP tendons with bonded steel strands achieved the highest load but it did not achieve the highest deflections. The highest deflection was achieved by H-0.085BS-0.153US at 4.27", which corresponds to an increase of 109% compared to U-0.153 deflection.

The unbonded tendons area and material were also investigated further in the hybrid beams. The results show that using CFRP tendon in the post-tensioning process with the same steel tendon diameter can achieve the same or higher capacity with a minor reduction in the deflection. For H-0.153BS-0.153US the capacity achieved was 32.8 kips at 3.89 in of deflection and when the 0.153 in^2 unbonded tendons was replaced by 0.11 in^2 CFRP tendons, the capacity was increased to 34.39 kips with a deflection of 3.11 in. In addition, the load-deflection behavior for the hybrid member did not change much when the unbonded tendons depth was switched with the bonded ones. Both beams maintained the same level of load and deflection.

The final comparison was made based on the prestressing technique (fully bonded, fully unbonded, Hybrid). The results show that although H-0.085BS-0.11UF-D achieved the highest capacity of 29.86 kips, it didn't maintain the same level of deflection as BB-0.085, UU-0.085 and H-0.085BS-0.085US-D. The deflection achieved by the CFRP hybrid beam was 72% less than the average deflection achieved by the other specimens in this group.

Table 4.11. Summary of Applied and Measured Mid-Span Deflections at Various Limit States

Beam Designation	$\Delta_{camber(B)}$ (in)	$\Delta_{camber(U)}$ (in)	$\Delta_{camber(Total)}$ (in)	P_{cr} (kips)	Δ_{cr} (in)	P_y (kips)	Δ_y (in)	$P_{py(B)}$ (kips)	$\Delta_{py(B)}$ (in)	$P_{py(U)}$ (kips)	$\Delta_{py(U)}$ (in)	$P_{(U)}$ (kips)	$\Delta_{(U)}$ (in)
H-0.085B-0.11UF-D	0.011	0.039	0.05	13.83	0.255	20.7	0.67	27.38	2.064	-	-	29.86	3.214
H-0.085B-0.085U-D	0.003	0.016		10.19	0.205	14.2	0.452	20.4	1.061	18.7	0.781	24.95	5.213
U-0.085	-			6.6	0.134	9.9		-	-	11.8	0.46	16.21	3.55
U0.153	-	0.019	0.019	6.5	0.138	12.8	0.607	-	-	16.35	1.51	17.96	2.034
H-0.085B-0.085U				12	0.315	21.8	0.66	17.2		20.1		24.29	4.765
H-0.085B-0.153U		0.015		10.57	0.192	21.4	0.632	25.6	1.549	27.2	2.045	30.63	4.278
H-0.153B-0.153U				13	0.227	22.4	0.732	31.5	2.186	31.05	3.76	32.8	3.89
U-0.11F-8ft	-			5	0.055	10.5	0.18	-	-	-	-	21.7	1.89
U-0.11F	-	0.022		6.1	0.1	9.19	0.641	-	-	-	-	18.29	2.33
U-0.19F	-			7.7	0.17	11.73	0.46	-	-	-	-	23.18	5.52
H-0.085B-0.11UF	0.010	0.016		11.9	0.162	18.43	0.91	19.2	0.969	-	-	27.16	3.894
H-0.153B-0.11UF				15.64	0.12	27.43	0.134	32.32	1.176	-	-	34.39	3.113
BB-0.085			0.033	10.09	0.26	17.5	0.586	24.24	1.511	25.98	3.524	26.89	5.63
UU-0.085	0.039	0.02	0.059	10.74	0.174	17.5	0.616	22.195	1.573	24.233	2.181	26.8116	5.803

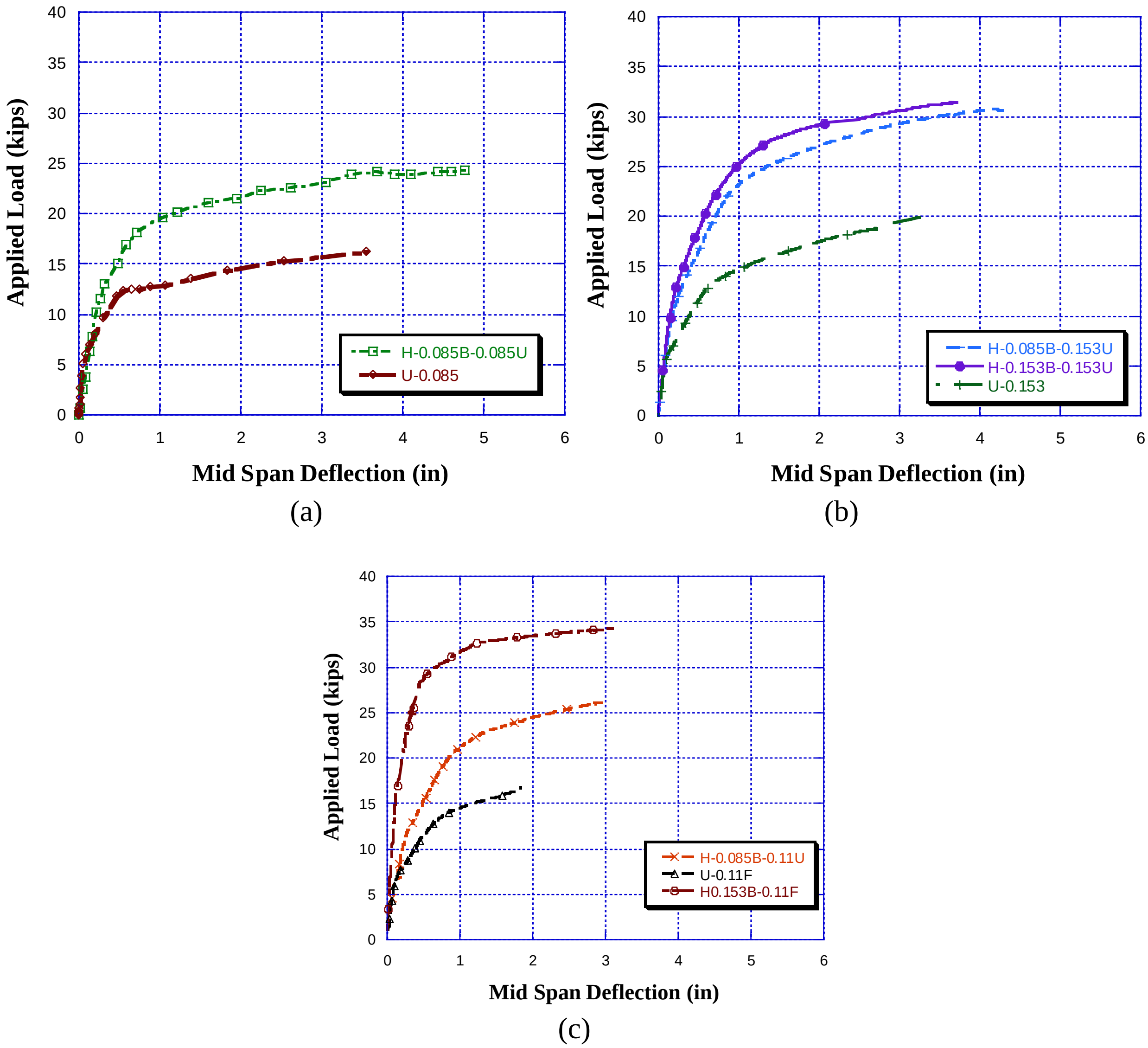

Figure 4.17. Effect of Bonded Tendons Area on Load-Deflection Behavior for Same Unbonded Tendon; (a) A_{psu} = 0.085 in^2, (b) A_{psu} = 0.153 in^2, (c) A_{psu} = 0.11 in^2

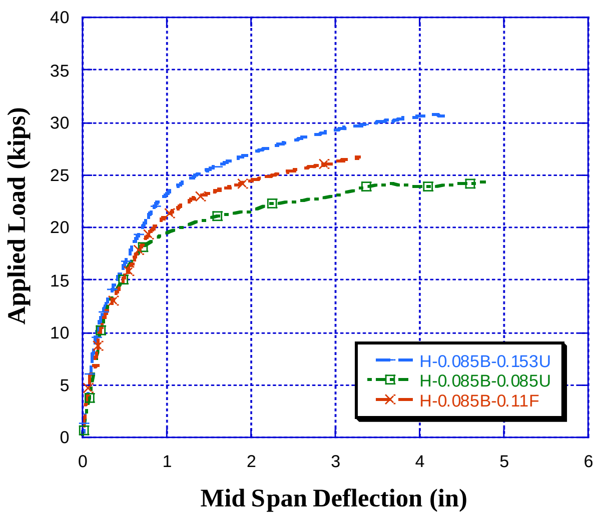

(a)

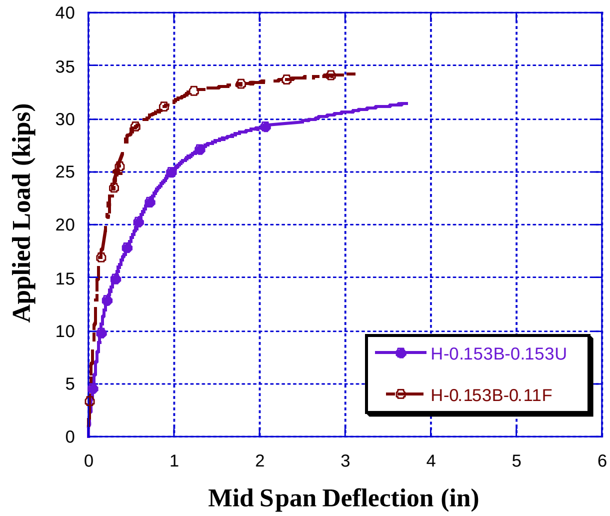

(b)

Figure 4.18. Effect of Unbonded Tendons Area (Hybrid Beams) on Load-Deflection Behavior for Same Bonded Tendon (a) A_{psb} = 0.085 in^2, (b) A_{psb} = 0.153 in^2

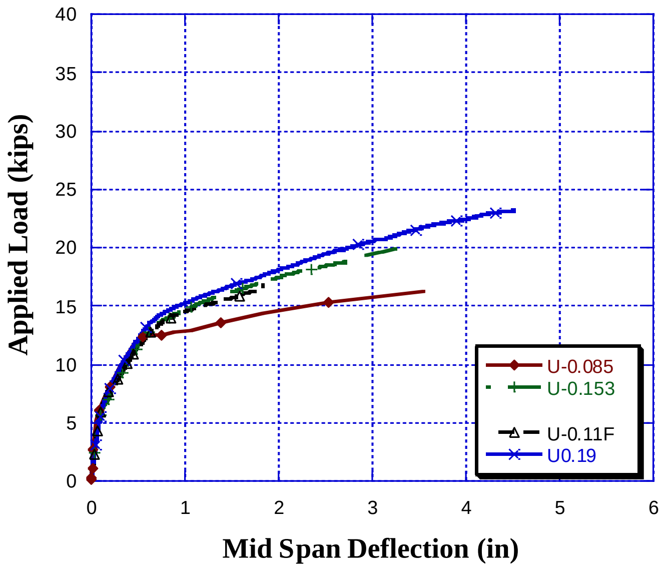

Figure 4.19. Effect of Unbonded Tendons Area (Unbonded Beams) on Load-Deflection Behavior

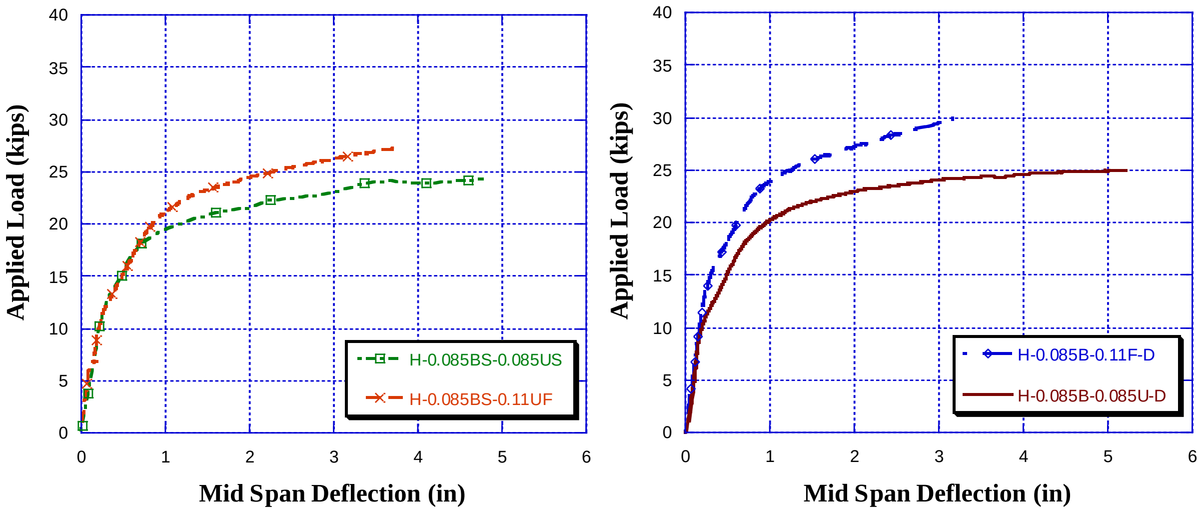

Figure 4.20. Effect of Unbonded Tendons Material (Steel/FRP) on Load-Deflection Behavior; (a) d_{psb} = 8.875 in, d_{psu} = 6.125 in, (b) d_{psb} = 7.5 in, d_{psu} = 8.875 in

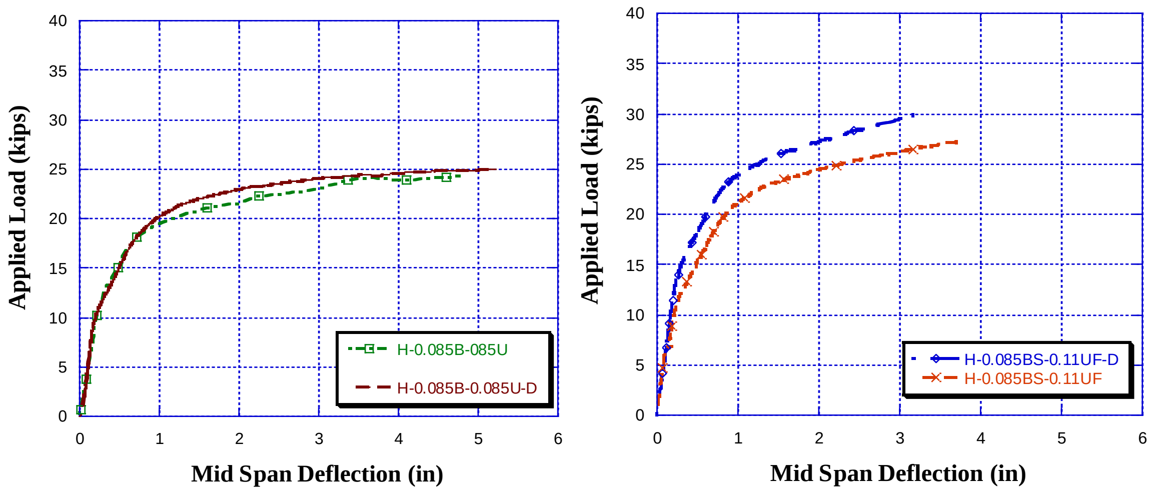

Figure 4.21. Effect of Tendons Depth (Both Bonded and Unbonded) on Load-Deflection Behavior (a) Steel Tendons, (b) CFRP Tendons

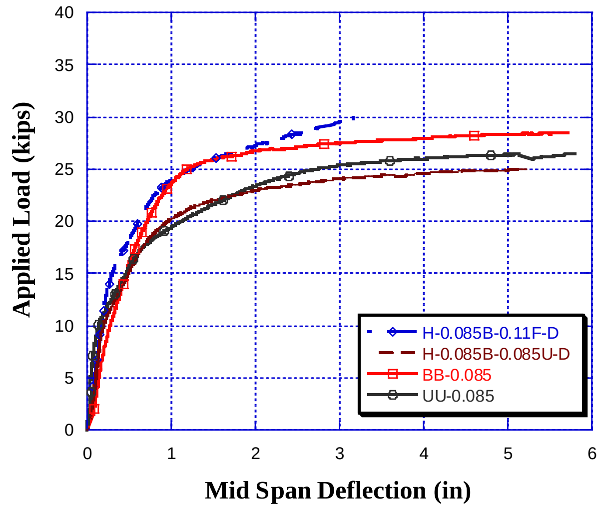

Figure 4.22. Effect of Hybrid Combination Compared to Fully Bonded and Unbonded on Load-Deflection Behavior

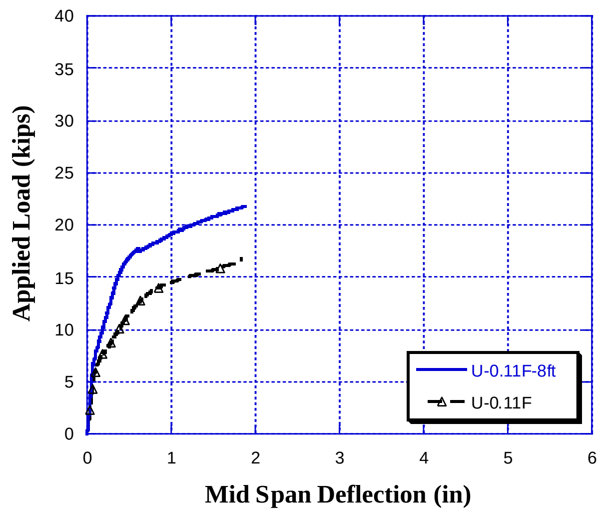

Figure 4.23. Effect of Beam Length on Load-Deflection Behavior

5. LIFE CYCLE COST ANALYSIS

5.1. Introduction

In this study, fiber reinforced self-consolidating concrete (FR-SCC) and fiber reinforced ferrocement (FR-FC) are utilized in repairing bridge concrete structure elements. Repairing the concrete structure elements using these types of advanced materials decreases the construction time, labor, and equipment needed on construction sites; and increases the service life of the structure up to 5-10 years. Fiber reinforcement improves the technical benefits of self-consolidating concrete (SCC) and ferrocement (FC) by providing crack bridging ability, higher toughness, and long-term durability.

To evaluate the cost-effectiveness of these new repair materials and technologies, both project-level and network-level economic evaluations are needed. Life Cycle Cost Analysis (LCCA) is such an effective economic-engineering decision-support solution. On the one hand, project-level LCCA analysis factoring in all costs incurred during the lifetime of a transportation asset, including future maintenance, repair and rehabilitation (MR&R), delays in traffic, and social-economic impacts. On the other hand, network-level LCCA analysis is needed as well because it evaluates different combinations of projects and treatments to yield maximum benefits in developing cost-effective investment strategies (Gao et al.).

By using LCCA approach, the objective of this section is to investigate whether prestressed concrete bridges utilizing FR-FC or FR-SCC repair techniques can represent a cost-effective design alternative to conventional concrete prestressed concrete bridges at both project- and network-level.

5.2. Literature Review

Follow FHWA (FHWA 2002, 1998, Patidar et al. 2007) and many State Highway Agencies (SHAs) guidelines, numerous LCCA studies have been applied to transportation assets such as highways or bridge structures. LCCA has also been performed on bridge beams or girders at the project level. For example, Eamon et al. (Eamon et al. 2012) conducted both deterministic and probabilistic LCCA on prestressed concrete bridge superstructures using black steel, epoxy-coated steel and carbon fiber reinforced polymer (CFRP) materials. Two bridge girder types, prestressed concrete box beams and prestressed AASHTO beams, three span lengths and high/low traffic volumes were tested. Maintenance and replacement activities of steel-reinforced bridges including superstructure replacement, deck and beam replacement, deck overlay, beam end repair, deck patch, and cathodic protection were considered. For CFRP bridges, it only requires deck shallow overlay and deck replacement. Their study found that although with a higher initial cost, CFRP application had a 95% probability of being less expensive than the other two alternatives during year 23-77. Liang et al. (Liang et al. 2007) presented various bridge LCCA cost models and illustrated detailed cost breakdown including design, production, construction, quality assurance, failure, maintenance, inspection, periodic repair or replacement, and capital benefit cost. They applied LCCA on two prestressed concrete bridges and proved that the analytical model is reliable that can be potentially used as an engineering decision making tool.

Based on NCHRP and The Asset Management Rule (the Rule) (Federal Highway Administration 2016), an ideal network-level model considering LCC is naturally a multi-objective optimization process that requires decision makers to evaluate the trade-offs between different conflicting objectives. It should take advantage of existing asset management system capabilities (Federal Highway Administration 2017), for instance, integrating project level information from existing databases to network level analysis. Table 5.1. Literature Review on Network-level Life Cycle Cost Models synthesizes several network-level LCCA models presented in NCHRP Reports, used by state DOTs, and proposed by researchers over the past two decades (Gao et al.). While not exhaustive, it provides a representative sample of recent research efforts. The purpose of Table 1 is to understand recent approaches used in for the network-level LCCA and to identify the research and development needs for applications involving new materials or technologies. Each model's objective function, time frame and searching algorithm were investigated and summarized.

Table 5.1 presents various multi-objective optimization-based models that produces equally-good solutions known as a "Pareto Front" in which no alternatives can improve one or more objectives without making at least one objective worse. Different objectives can be either treated as separate functions without any preference before the optimization process (Liu and Frangopol 2005), or can be converted into a single-objective function (i.e. a single utility function) with subjective input (Marzouk and Omar 2013, Allah Bukhsh et al. 2018). An increasing trend is the usage of probabilistic approach is shown (Bryce et al. 2014, O. Swei, J. Gregory, and Kirchain 2015, Marzouk and Omar 2013, Yeo, Yoon, and Madanat 2010) in the last decade to account for the uncertainties. For instance, Bryce et al. (Bryce et al. 2014) treated the expected energy consumption probabilistically and pointed out that a probabilistic approach should be applied when the variable uncertainties may be significant. Table 5.1. Literature Review on Network-level Life Cycle Cost Models also showed that less than half of the studies considered user cost, and only three studies take social cost (i.e. from environment impacts) into account. In addition, a few studies (Sobanjo and Thompson 2007, Yeo, Yoon, and Madanat 2010, Patidar 2007) considered project- and network-level integration so information from existing asset management systems can be directly used as network-level inputs.

Ideally, a project-level LCCA model should be capable of quantifying the benefit and cost brought by the new materials or technologies, including agency, user and social costs, while a network-level optimization model should consider multiple performance measures, effect of time, uncertainty, outcome interpretation, and integration between project- and network-level (Gao et al.). Current practices meet one or some of the goals, but there is a need to develop a holistic and comprehensive tool that meets all of needs.

Table 5.1. Literature Review on Network-level Life Cycle Cost Models

Study	Year	Asset Type	Objective(s)	Cost Component	Method	Time Frame
Bryce et al. (Bryce et al. 2014)	2014	Pavement	min (maintenance cost), max (condition), min (energy consumption)	agency cost and social impact	Pareto front-based approach	3-year
Swei et al. (O. Swei, J. Gregory, and Kirchain 2015)	2015	Pavement	Min (excess fuel consumption)	Only agency cost	Simple heuristic approach	15-year
Zhang et al. (Zhang, Keoleian, and Lepech 2012)	2012	Pavement	Min (life cycle energy consumption), min (GHG emissions), min (costs)	Agency and social cost	Backward Dynamic Programing	20-year
Marzouk & Omar (Marzouk and Omar 2013)	2013	Sewer	min (cost), max (condition), max (extended network service life)	Only agency cost	Generic Algorithm	50-year
Liu & Frangopol (Liu and Frangopol 2005)	2005	Bridge	Max (overall performance of a bridge network), min (maintenance cost)	Only agency cost	Generic Algorithm	30-year
Bukhsh et al. (Allah Bukhsh et al. 2018)	2018	Bridge	Max (condition index), min (agency cost), min (user delay cost), min (environmental cost)	Agency, user and social cost	Utility Theory	Not Applied
Yeo et al. (Yeo, Yoon, and Madanat 2010)	2010	Pavement	min (total system cost)	Agency cost	Generic Algorithm	40-year
Florida DOT (Sobanjo and Thompson 2007)	2007	Bridge	min (Life cycle cost)	Agency and user cost	Incremental benefit/cost algorithm	10-year
Indiana DOT (Sinha et al. 2009)	2009	Bridge	Min (Overall benefits or effectiveness)	Agency and user cost	Dynamic/ Integer linear programming /Markov chain	10-year

5.3. Stochastic Multi-Objective Optimization-based LCCA Framework

Consider an infrastructure system composed of n independent facilities with different serviceability, traffic loads, etc. A "project candidate" in this study is defined as a life-cycle activity profile that contains a sequence of M&R activities for a transportation facility over certain analysis period. The proposed method aims to develop a two-level bottom-up approach based on LCC considerations. In the project-level, we first find "project candidates" -- all feasible M&R strategies for each facility based on project-level constraints, such as the facility's maximum traffic load or minimum acceptable serviceability and calculate the associated cost for each candidate. Secondly, we solve the network-level optimization to find the best combination of projects to meet network-level goals by choosing among project candidates found in the project-level model. Various economic and engineering models with optimization algorithms (i.e. Evolutionary Algorithm) are combined in the proposed approach to balance the trade-off between objectives and arrive at the optimum or near-optimum life cycle strategy. In addition, by connecting the two-level approach with an existing database as well as empirical deterioration models for the facilities, we are able to establish an integrated project- and network-level LCCA model framework as illustrated in Figure 5.1.

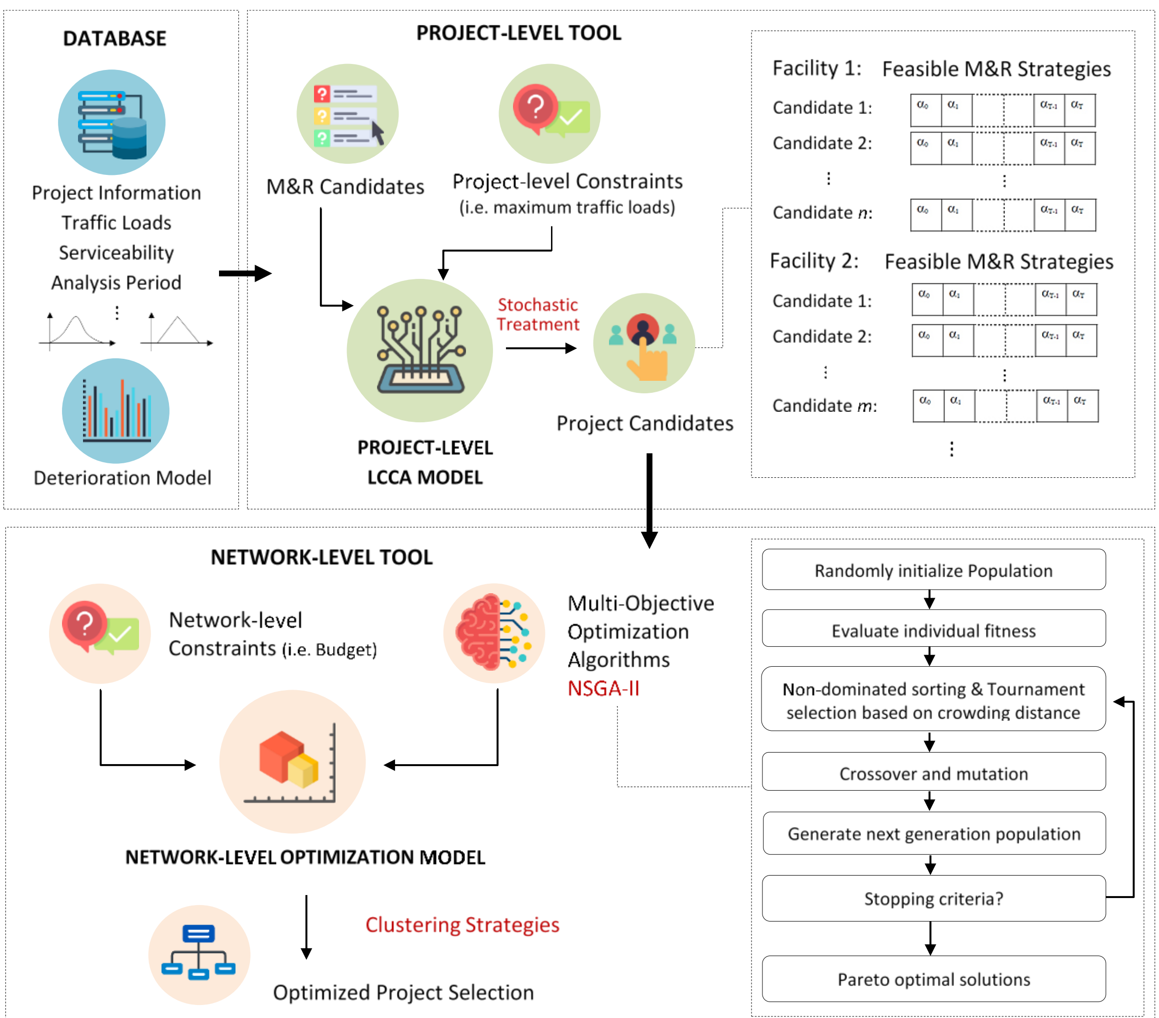

Figure 5.1. An integrated project- and network-level LCCA model framework.

5.3.1. Project-level LCCA Model

Let's denote t as the year and T as the analysis period. $a_t \in \{0,1,2...m\}, \mathrm{m} \in \mathbb{N}$ is a non-negative integer representing the type of M&R activity to be scheduled at year t. a_t equals zero if no activity is to take place that year. For example, if bridge project A has three types of activities (0,1,2) that stands for "no action" "repair" and "replacement", then $a_{20} = 2$ means at year 20, a type 2 activity "replacement" is scheduled. The M&R strategy for a project becomes a sequence of a_t.

The proposed project-level LCCA model considers three cost components: agency cost, user costs and social cost. User cost in the proposed methodology includes a Traffic Delay Cost (TDC) model using deterministic queueing approach (Ozbay and Kachroo 1999), a Vehicle Operation Cost (VOC) adopted from NCHRP Report 133 method and FHWA's guideline on work zone road user costs (Mallela and Sadavisam 2011), and a Crash Risk Cost (CRC) model (Bonstedt 2010, Ozbay, Yanmaz-Tuzel, et al. 2007). Social cost (SC) has an air pollution module (Ozbay, Bartin, et al. 2007) and can be extended to include other costs from noise or energy consumption. Only the differential user and social costs occurring during work zone periods are considered in this approach. Weights are assigned to different costs to mimic the actual decision-making process used in many agencies where the agency costs usually get the highest weight (Jawad 2003). For each M&R strategy j of facility i, its net present value (NPV) is calculated as follows:

$$\mathrm{NPV} = \sum_{t=0}^{T} \frac{w_1(AC_t(a_t) - \mathrm{SV_t}) + w_2(TDC_t(a_t,V_t) + VOC_t(a_t,V_t) + CRC_{(t)}(a_t,V_t)) + w_3 \cdot SC_t(a_t,V_t)}{(1+r)^t} \quad (1)$$

where,

t = the year at which the cost is incurred (years)
T= analysis period (years)
r = discount rate (decimals)
a_t = a non-negative integer representing the type of maintenance & rehabilitation (M&R) activity to be scheduled at year t and equals to zero if no M&R action is to take place, a_t is bound by deterioration function $f(CR_t)$, where CRt is the condition rate at year t.
V_t = AADT at year t (vehicles/day) and $V_t \le Max(\mathrm{AADT})$
$AC_t(a_t)$, $TDC_t(a_t,V_t)$, $VOC_t(a_t,V_t)$, $CRC_t(a_t,V_t)$, $SC_t(a_t,V_t)$ are the agency cost, traffic delay cost, vehicle operation cost, crash risk cost, and social cost at year t ($); all are dependent on M&R activity a_t. Traffic delay, vehicle operation, crash risk, and social cost are also subject to traffic volume Vt
$\mathrm{SV_t}$ = the salvage value, it only occurs at the end of the analysis period T ($)
w1, w2, w3 are the weight factor of agency cost, user cost, and social cost

Since the technical performance, initial construction cost, timing and cost of M&R activity, and disposing of a new-material structure are usually less certain than those for conventional materials, these variabilities can greatly affect the final solutions. Therefore, stochastic treatments - Monte Carlo simulations are applied when calculating all cost components. The final output of the project-level tool is a set of feasible project candidates that contains a sequence of M&R activity a_t and associated costs. It is worth mentioning that different candidates of the same facility may have the same type of M&R activities, but because these activities are scheduled for different years, their costs will be different. Traffic growth is bounded by the maximum allowable traffic that can pass through the facility, so this value cannot grow infinitely and lead to unrealistic user or social cost. Furthermore, the maximum allowable year for the first rehabilitation/replacement action depends on the minimum acceptable serviceability of the facility– if a facility's estimated serviceability at year t is less than a certain threshold, a rehabilitation/replacement activity is assumed to be scheduled immediately for the next year t+1. Each candidate after this year becomes infeasible. Consequently, each facility has a different number of feasible candidates.

5.3.2. Network-Level Multi-Objective Optimization Model

Assuming that all facilities are independent and given a set of constraints (i.e. budget), the network-level optimization can be formulated as a multi-choice, multi-dimensional knapsack problem (MCMDKP). Let's denote $M_i = \{0,1,2,...\}$ to be the feasible project candidates for facility i where $1 \le i \le n$. x_{ij} is the decision variable and equals to 1 if candidate j of facility i is selected ($j \in M_i$). Two objectives are considered in this study. The first objective is to minimize the total LCC of selected project candidates. The second objective is to consider facility importance. For example, bridges carrying heavier traffic may get higher priority than others as they are more sensitive to potential failure. Therefore, traffic loads are used to represent facility importance. Both objectives are normalized so they are comparable. The network-level optimization problem can be formulated as follows:

$$\text{Minimize} \sum_{i=1}^{n} \sum_{j \in M_i} NPV_{ij} x_{ij} \tag{2}$$

$$\text{Maximize} \sum_{i=1}^{n} \sum_{j \in M_i} AADT_i x_{ij} \tag{3}$$

subject to:

$$B_l \le \sum_{i=1}^{n} \sum_{j \in M_i} AC_{ij} x_{ij} \le \mathrm{B}_u \tag{4}$$

$$\sum_{j \in M_i} x_{ij} \le 1, \qquad (1 \le i \le n) \tag{5}$$

$$\sum_{i=1}^{n} \sum_{i \in M_i} x_{ij} \le S \tag{6}$$

$$x_{ij} = 0 \text{ or } 1 \tag{7}$$

where,

$x_{ij} = 1$ if candidate j of bridge i is selected, $x_{ij} = 0$ otherwise.

NPV_{ij} = Net Present Value of candidate j for bridge i

$AADT_i$ = Current annual average daily traffic of bridge i

CR_{0i} = Current condition rating of bridge i

AC_{ij} = Agency cost of candidate j for bridge i

B = Budget ($)

S = Maximum number of candidates selected

NCHRP Report 590 (Patidar et al. 2007) pointed out that besides a budgetary ceiling, considering a minimum budget is also necessary in the optimization problem. Hence, a lower bound of the budget is considered to ensure at least a certain percentage of the budget will be utilized. In addition to the monetary limitation, a maximum number of selected project candidates are determined in Equation (6) to represent agency resource limitations (i.e. maximum number of construction contractors an agency can have in a certain time horizon). Equation (7) is to make sure every facility will have only one project candidate (a sequence of M&R actions) selected.

Various optimization algorithms have been applied in long-term infrastructure management such as linear programming or dynamic programming. Evolutionary algorithms like Generic Algorithm (GA) based on Darwin's evolution theory have also gained recognition in many engineering applications. For the proposed network-level optimization model, the Non-dominated Sorting Genetic Algorithm II (NSGA-II) (Deb et al. 2002) is employed to obtain the Pareto optimal solutions. Steps of NSGA-II can be found in Figure 5.1. NSGA-II has been proven to be an efficient Multi-objective evolutionary algorithm that maintains population diversity and excellent individuals (Yu et al. 2015) and has been used in transportation asset management (Bai et al. 2015).

However, instead of a single solution, multi-objective optimization usually produces many equally good solutions, making it complicated to interpret the outcome. Furthermore, each managing agency may have additional performance measures besides minimizing cost and giving priority to important facilities. To solve these problems, we propose to have one more step after getting the Pareto-optimal solutions – applying multiple clustering strategies based on additional preferences. Additional preferences may include network-level serviceability requirement, less risky selections or best utilization of the budget. The best solutions from each cluster will give decision makers clearer insight into the outcome and narrow down the selections to a few optimal and sub-optimal solutions. More details about the project-level and network-level model can be found in (Gao et al.).

5.4. Structure Considered

Bridges with prestressed concrete girders are considered for the applications of the proposed repair techniques. A unified database is built for New Jersey includes roadway information, Weigh-in-Motion (WIM) Data from 81 WIM stations, traffic data from different sensors of NJDOT, bridge data from National Bridge Inventory (NBI) that contains the locations and the properties of 6918 bridges in NJ since 1992. Next, a subset of bridges (500 bridges) is extracted from the unified database based on National Bridge Inventory Code Item 43, Structure Type of main spans (Table 5.2). Based on the code, bridges with STRUCTRE_KIND_043A =5 or 6 and STURCTURE_TYPE_043B = 2 or 3 or 5 or 6 or 14 or 21 are selected.

Table 5.2. National Bridge Inventory Code Item 43 - Structure Type, Main (Administration 1995)

Code	STRUCTURE_KIND_043A	Code	STURCTURE_TYPE_043B
1	Concrete	1	Slab
2	Concrete continuous	2	Stringer/Multi-beam or Girder
3	Steel	3	Girder and Floorbeam System
4	Steel continuous	4	Tee Beam
5	Prestressed concrete	5	Box Beam or Girders - Multiple
6	Prestressed concrete continuous	6	Box Beam or Girders - Single or Spread
7	Wood or Timber	7	Frame (except frame culverts)
8	Masonry	8	Orthotropic
9	Aluminum, Wrought Iron, or Cast Iron	9	Truss - Deck
0	Other	10	Truss - Thru
		11	Arch - Deck
		12	Arch - Thru
		13	Suspension
		14	Stayed Girder
		15	Movable - Lift
		16	Movable - Bascule
		17	Movable - Swing
		18	Tunnel
		19	Culvert (includes frame culverts)
		20	Mixed types
		21	Segmental Box Girder
		22	Channel Beam
		00	Other

Because the NBI data does not provide the exact number of girders, therefore, two methods were proposed to estimate the number of girders for each bridge. Method 1 assumes the girder size can be incorporate with the minimum depth given by AASHTO LRFD Table 2.5.2.6.3-1 (Table 5.3). However, this method does not consider the material strength. The number of girders is in incorporated with the span-to-depth ratio. We usually decide on the girder depth and girder spacing based on the span length and width of the bridge. Over the years, although engineers have developed certain simple thumb of rules on decision making that gives a start to design (AASHTO), based on the experiences in the real design, the minimum girder depth usually does not control the selection of the girder size. As a result, the estimation tends to be small.

Table 5.3. AASHTO LRFD Table 2.5.2.6.3-1 Traditional Minimum Depths for Constant Depth Superstructures.

Superstructure		Minimum Depth (Including Deck) When variable depth members are used, values may be adjusted to account for changes in relative stiffness of positive and negative moment sections	
Material	Type	Simple Spans	Continuous Spans
Reinforced Concrete	Slabs with main reinforcement parallel to traffic	$\frac{1.2\ S+10}{30}$	$\frac{S+10}{30} \geq 0.54$ ft.
	T-Beams	$0.070L$	$0.065L$
	Box Beams	$0.060L$	$0.055L$
	Pedestrian Structure Beams	$0.035L$	$0.033L$
Prestressed Concrete	Slabs	$0.030L \geq 6.5$ in.	$0.027L \geq 6.5$ in.
	CIP Box Beams	$0.045L$	$0.040L$
	Precast I-Beams	$0.045L$	$0.040L$
	Pedestrian Structure Beams	$0.033L$	$0.030L$
	Adjacent Box Beams	$0.030L$	$0.025L$
Steel	Overall Depth of Composite I-Beam	$0.040L$	$0.032L$
	Depth of I-Beam Portion of Composite I-Beam	$0.033L$	$0.027L$
	Trusses	$0.100L$	$0.100L$

The second method is based on the idea that the girder size and girder spacing can be incorporated with Calibration of AASHTO LRFD Concrete Bridge Design Specifications for Serviceability (Wassef et al. 2014). In this method, the following assumptions are made: 1) The concrete strength is 6 ksi, and 2) in order to conservatively estimate the material volume needed for repair, the girder spacing is taken as the smallest (6 ft) from the report.

5.4.1. Hypothetical Project-level LCCA Example

This section illustrates a hypothetical project-level LCCA using one bridge from New Jersey. The purpose is to evaluate the cost difference between several different alternatives. The repair type chosen usually depends on a project-by-project basis, but for the simplification of this hypothetical example, the following assumptions are made:

- FR-SCC and FR-FC layer will be applied at the bottom of each concrete girder after the cover peeled. On average, the layer is about 2 inches.
- FR-SCC needs forms around the girder (less labor but more material and pumps to pump the material) and FR-FC can be applied without forms (more labor).
- The material unit price for girder repair using conventional concrete, FR-SCC layer, FR-FC layer is $91.05, $106.05, $88.0 per cubic yard. The material unit price is assumed to account for 66% of the construction unit cost (Barker 2017).
- The repair and rehabilitation schedule for the reference AASHTO prestressed I-bridge using conventional repair approach is assumed to be 30 years and 52 years (Weyers et al. 1993, Boatman 2010).
- The time needed for repair activities (conventional repair technique, FR-FCC and FR-FC) is assumed to be two weekends utilizing off-peak traffic hours.
- Social cost, such as air pollution cost is relatively small in this case, therefore only agency and user costs are considered. Only the costs associated with repair and rehabilitation activities are considered (exclude costs occurred during normal operations) .
- The repair activities (i.e. lane/bridge closure) using FR-SCC/FR-FC repair techniques will have the same impact level on traffic delay, vehicle operation or crash risk.
- Since our focus is to evaluate the effectiveness of the repair techniques, the service life extension benefit for rehabilitation is only considered in the salvage value in this case study.

Based on the laboratory results, the girders service life will be extended for a few years (5-10 years). Therefore, five scenarios are examined: 1) A reference conventional concrete used for both girder repair and rehabilitation (Conventional), 2) FR-SCC for both girder repair and rehabilitation with 5 year service life extension (FR-SCC (+5)), 3) FR-SCC for both girder repair and rehabilitation with 10 year service life extension (FR-SCC (+10)), 4) FR-FC for repair and FR-SCC for rehabilitation with 5 year service life extension (FR-FC+FR-SCC (+5)) , and 5) FR-FC for repair and FR-SCC for rehabilitation with +10 year service life extension (FR-FC+FR-SCC (+10)). Stochastic treatments are applied using Monte Carlo simulation (5000 runs each). Discount rate and material unit price are treated probabilistically. Bridge and project-level LCCA inputs are listed in Table 5.4.

The results of the probabilistic project-level LCCA are summarized in Table 5.5 and Table 5.6. The life cycle cost saving using FR-SCC for both repair and rehabilitation with 5-year service life extension and FR-FC for repair and FR-SCC for rehabilitation with 5-year service life extension are relatively small (3.9% to 4.4%) compare to conventional repair approach. Applying FR-SCC for both repair and rehabilitation with 5-year service life extension is 13.8%, 11.7%, and 12.5% less expensive compared with the conventional approach in terms of agency, user and weighted life cycle cost, respectively. FR-FC for repair and FR-SCC for rehabilitation with 10-year service life extension has the best savings among the five alternatives (15.1%, 11.7% and 13% for agency, user and weighted life cycle cost). Figure 5.2 illustrates the probability density function (PDF) and cumulative distribution function (CDF) of the five alternatives. The results are in agreement with Table 5.5 and Table 5.6 that FR-FC for repair and FR-SCC for rehabilitation with 10-year service life extension has the least costs (solid black lines). The differences between using FR-SCC for both repair and rehabilitation and FR-FC for repair/FR-SCC for rehabilitation with the same number of years' service life extension are relatively small (Dashed black vs solid grey line and solid black vs solid green line).

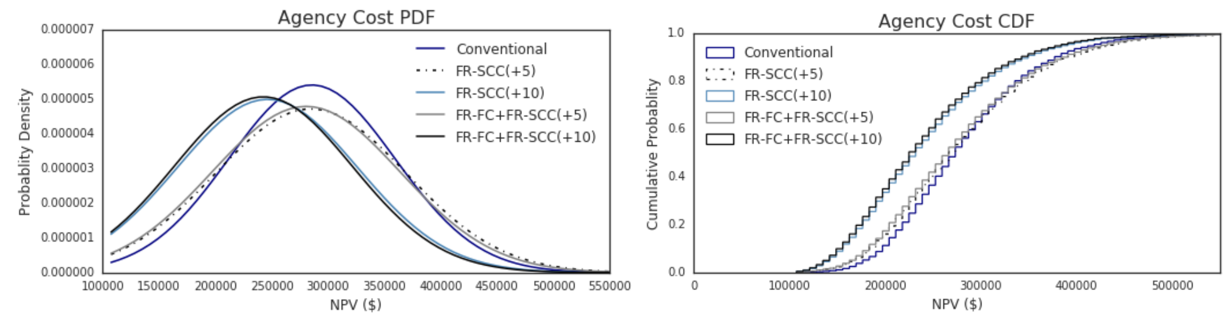

(a)

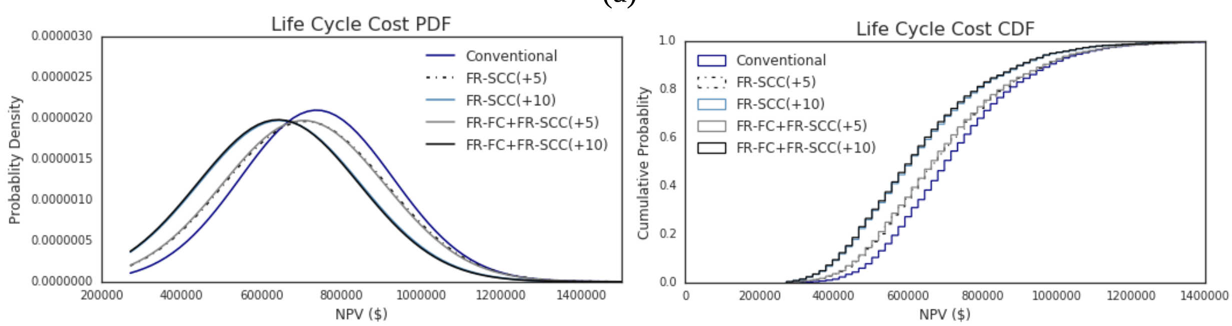

(b)

Figure 5.2. PDF and CDF Plots for Project-Level LCCA; (a) PDF and CDF for Agency Cost and (b) PDF and CDF for Weighted Life Cycle Cost

Table 5.4. Project-Level LCCA Inputs

Analysis period	75 years	Girder depth	19.4 inch
Discount rate	N (3%, 0.05%)	Structure width	208 feet
Material unit price (Conventional) (per yd3)	N ($91.05, $4.5)	Estimated number of girders	32
Material unit price (FR-SCC) (per yd3)	N ($106.05, $10.6)	AADT	118,157 vehicles per day
Material unit price (FR-FC) (per yd3)	N ($88.0, $8.8)	Truck percentage	1.55%

Table 5.5. Project-Level LCCA Results

Alternative	Conventional		FR-SCC (+5)		FR-SCC (+10)		FR-FC+FR-SCC (+5)		FR-FC+FR-SCC (+10)	
	Mean	Std	Mean	Std	Mean	Std	Mean	Std	Mean	Std
Agency Cost	$285,644	$73,849	$284,762	$84,629	$246,197	$79,977	$280,485	$83,374	$242,490	$78,837
User Cost	$1,508,482	$391,098	$1,416,210	$403,945	$1,331,441	$414,708	$1,416,210	$403,945	$1,331,441	$414,708
Weighted LCC*	$738,189	$190,273	$709,625	$203,405	$645,630	$202,384	$705,348	$202,481	$641,923	$201,521

*As a common practice, a 0.3 user cost weight factor is applied when calculating weighted LCC values.

Table 5.6. Cost Difference Compare with Conventional Repair Approach

	FR-SCC (+5)	FR-SCC (+10)	FR-FC+FR-SCC (+5)	FR-FC+FR-SCC (+10)
Agency Cost	-0.3%	-13.8%	-1.8%	-15.1%
User Cost	-6.1%	-11.7%	-6.1%	-11.7%
Weighted LCC	-3.9%	-12.5%	-4.4%	-13.0%

5.4.2. Hypothetical Network-level LCCA Example

Not like the project-level analysis, network-level LCCA aims to find an optimal or near-optimal set of projects that need to be repaired or rehabilitated while meeting network-level goals such as agency budget or minimum acceptable network condition ratings. In this section, a probabilistic network-level example for bridge girder are conducted with two alternatives: conventional repair technique and FR-FC+FR-SCC (+10). The later is the best alternative identified from the project-level analysis. We first sorted the bridges with prestressed concrete girders and extracted the worst 15 bridges that may need immediate girder repair or rehabilitation (Table 5.7). Let's use the first four digits to represent the bridge ID and the next two digits to represent the year of the first repair/rehabilitation activity, for example, "bridge 0 - year 1" project candidate is denoted as ('0000','01').

Table 5.7. Bridges Selected for Network-Level LCCA Analysis

ID	ADT	STR. LEN (FT)	DECK WIDTH (FT)	SUPER CR*	Truck%	GIRDER DEPTH	#GIRDER	APPLICABLE GIRDER SIZE
1	18948	48.872	74.128	4	4	17.6	18	BI-48
2	16493	56.088	70.848	5	4	20.2	17	BI-48
3	3678	61.992	36.408	5	4	22.3	9	BII-36
4	4572	63.96	23.944	5	3	23	5	BII-36
5	1374	21.976	43.624	5	3	7.9	10	BI-48
6	5328	39.032	45.92	5	4	14.1	11	BI-48
7	24828	22.96	83.968	5	4	8.3	20	BI-48
8	17585	43.952	70.192	5	4	15.8	17	BI-48
9	9090	30.832	46.904	5	4	11.1	11	BI-48
10	12430	56.088	48.544	5	3	20.2	12	BI-48
11	77092	50.84	112.832	5	5	20.5	18	AASHTO II
12	8487	87.904	60.352	5	4	40.5	10	AASHTO IV
13	5680	45.92	38.704	5	3	16.5	9	BI-48
14	6050	30.832	33.128	4	3	11.1	8	BI-48
15	13245	46.904	78.064	5	4	16.9	19	BI-48

*Superstructure condition rating

For each probabilistic run, the network-level optimization model generates various pareto-optimal solutions where each solution is a combination of different project candidates. Due to the stochasticity of input parameters and the NSGA-II searching procedure, the pareto-optimal solutions of each run may be different. The final network-level optimization model output contains all pareto-optimal solutions that ever exist in any of the runs and their selection probabilities are computed. Selection probability indicates how many times this solution is selected as a pareto-optimal solution during all probabilistic runs. A solution with lower selection probability means a relatively riskier solution in comparison to a solution with higher selection probability. The network-level model specifications are shown as follows:

- Agency budget (for sum of the agency costs): 1.6 Million Dollars
- Network objectives: minimize the total LCC and maximize facility importance of selected project candidates. Traffic volume carried by the bridge is used as an approximation for facility importance.
- Maximum number of projects in each project set: 5

- Number of probabilistic runs: 100
- Number of NSGA-II generations: 50 (50 generations x 100 probabilistic runs =5,000 generations in total)
- The time horizon for LCC calculations: 75 years
- Year-10 evaluation of average network conditional rate is computed as an additional network-level performance measure.

The final model generates 309 and 99 pareto-optimal solutions using conventional repair technique and FR-FC+FR-SCC (+10), respectively. Figure 5.3 presents the first 50 solutions ranked by their selection probabilities for each alternative. In this example, because the 15 bridges selected are all under fair or poor condition, the final project set of the bridges indicates they need immediate repair/rehabilitation (with '01' after each bridge ID)

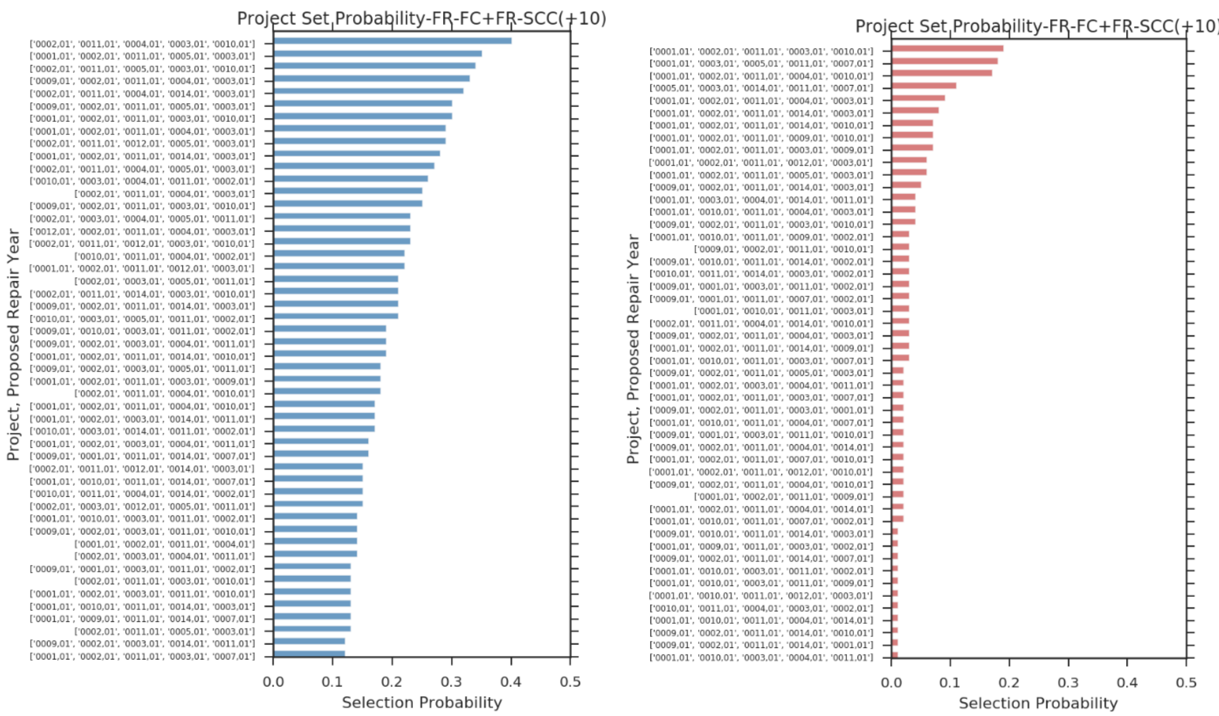

Figure 5.3. Network-Level Optimization Model Results

Next, two clustering strategies are applied to better interpret the results. The first strategy is to best utilize the available budget, so the remaining budget is minimized. The second strategy is to maximize the average network condition rate (evaluated at the end of a 10-year planning horizon), therefore it can meet the agency's performance goals. An efficient unsupervised learning algorithm, K-means, is used to cluster the pareto-optimal solutions into three clusters. Figure 5.4 and Figure 5.5 illustrates the graphic representation of the clustering results. Network performance measures of the top solution (project set) in each cluster are listed in Table 5.8 including total agency cost, total life cycle cost, total traffic loads, average network condition rating, remaining budget and selection probability. The results are for the mean condition - the average of the stochastic variables.

Our findings provide additional support for the benefit of using the proposed new repair technique on the network-level. For example, for the same project set, FR-FC+FR-SCC (+10) requires lower agency cost and lower LCC (reference point 1 and 2). Bridges selected using conventional repair alternative (reference point 1) has a total agency cost of $1.53 million and a total LCC of $4.92 million while for the same set of selected bridges, FR-FC+FR-SCC (+10) alternative only costs $1.21 million and $4.73 million in agency cost and LCC (reference point 2), respectively.

For similar budget levels, FR-FC+FR-SCC (+10) allows decision-makers to select bridges with higher traffic loads (reference point 3 and 4). Reference point 3 and 4 both have similar budget levels ($1.24 Million and $1.26 Million), but the bridges selected by reference point 4 carry a total of 128,944 vehicles per day compare to 103,443 vehicles per day of the bridges selected using conventional repair technique.

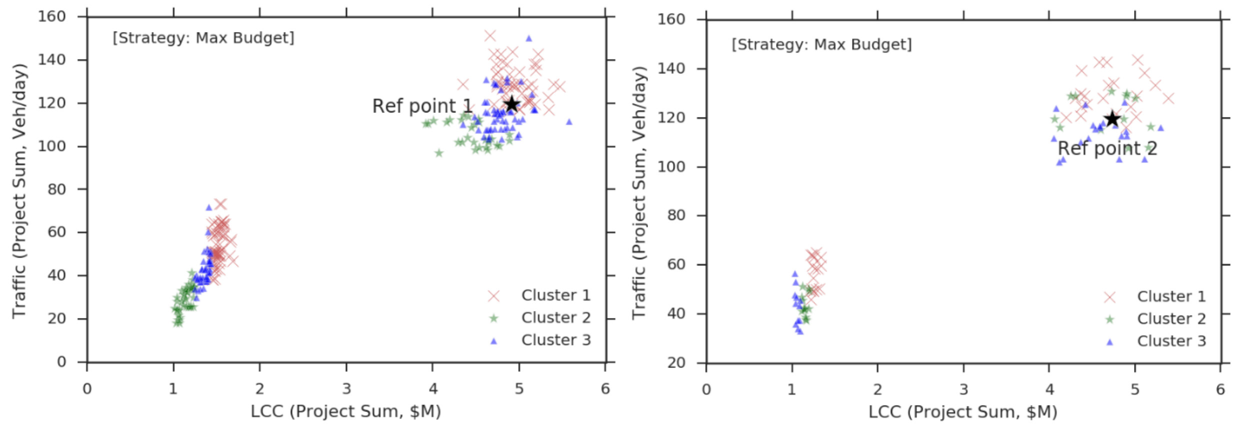

(a) (b)

Figure 5.4. Strategy 1: Maximizing Available Budget; (a) Conventional and (b) FR-FC+FR-SCC (+10)

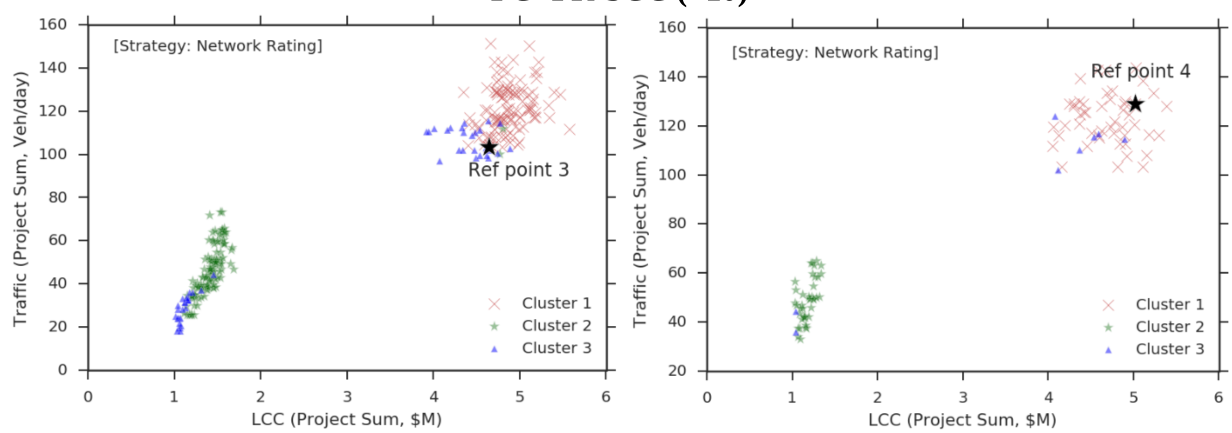

(a) (b)

Figure 5.5. Strategy 2: Maximizing Network Condition Ratings; (a) Conventional and (b) FR-FC+FR-SCC (+10)

Table 5.8. Clusters based on Maximizing Network Condition Rating and Available Budget – Top Solution in Each Cluster

Strategy 1	Maximum Budget: Conventional repair technique							
	Project Set	Agency Cost (Sum, $M)	LCC (Sum, $M)	Traffic (Sum, 1000 Veh/day)	Avg Net CR	Remaining Budget	Selection Probability	Cluster
	[0002, 0011, 0004, 0003, 0010]	1.244743	4.641813	103.443752	5.966324	0.355257	0.4	1
	[0002, 0011, 0012, 0005, 0003]	1.226406	1.226679	30.093091	5.964655	0.373594	0.29	2
Ref point 1	[0001, 0002, 0011, 0003, 0010]	1.513493	4.919365	119.638668	5.966324	0.086507	0.3	3
	Maximum Budget: FR-FC+FR-FCC repair technique							
	[0001, 0003, 0005, 0011, 0007]	1.027522	1.027936	56.5156	5.964655	0.572478	0.18	1
	[0001, 0002, 0011, 0012, 0003]	1.150773	1.15113	41.990946	54.964655	0.449227	0.06	2
Ref point 2	[0001, 0002, 0011, 0003, 0010]	1.212223	4.736038	119.638668	5.966324	0.387777	0.19	3
Strategy 2	Network Rating: Conventional repair technique							
	Project Set	Agency Cost (Sum, $M)	LCC (Sum, $M)	Traffic (Sum, 1000 Veh/day)	Avg Net CR	Remaining Budget	Selection Probability	Cluster
	[0002, 0011, 0004, 0003]	1.050248	1.050455	19.707826	5.694358	0.549752	0.25	1
	[0001, 0002, 0011, 0005, 0003]	1.405864	1.406257	41.689269	5.964655	0.194136	0.35	2
Ref point 3	[0002, 0011, 0004, 0003, 0010]	1.244743	4.641813	103.443752	5.966324	0.355257	0.4	3
	Network Rating: FR-FC+FR-FCC repair technique							
	[0009, 0002, 0011, 0010]	1.038166	4.363978	110.248833	5.696027	0.561834	0.03	1
	[0001, 0003, 0005, 0011, 0007]	1.027522	1.027936	56.5156	5.964655	0.572478	0.18	2
Ref point 4	[0001, 0002, 0011, 0014, 0010]	1.260229	5.023135	128.944411	5.966324	0.339771	0.07	3

6. SUMMARY AND CONCLUSIONS

6.1. FR-SCC and FR-FC Strengthened Beams

This project presents the results of 44 RC beams strengthened in flexure with FR-F and FR-SCC laminates with different sizes of stirrups, fibers type and contents, mesh layers depth and type of reinforcement. Based on the initial results of this on-going study, the following observations and conclusions can be made:

- The use of FR-SCC and FR-F in strengthening beams that are deficient in flexure is effective in increasing the cracking load as well as the ultimate load.
- Using any of the proposed laminates, additional layers of meshes would result in higher ultimate and cracking capacities.
- The increase in the fibers percentages in the FR-FC and FR-SCC layers, in addition to the steel reinforcement show excellent improvement of the flexural capacity of the repaired RC beam.
- Combining micro fibers with macro PPF or steel fibers in the laminate reduces the crack width and increases the number of crack prior to failure
- The effect of stirrup sizes was pronounced when using FR-FC compared to FR-SCC due to the higher workability and flowability of the SCC mixes that creates a stronger bond with the exposed steel stirrups.

6.2. Hybrid Prestressed Beams

Based on the current experimental investigation of the hybrid prestressed beams, the following conclusions can be drawn:

- Hybrid beams in prestressed concrete shows great potentials in segmental bridge systems that could allow the use of CFRP as non-corrosive material with the use of bonded strands that is embedded in concrete
- The use of CFRP as a unbonded tendons in hybrid girders increase the ductility of the member in terms of the spacing, with and number of cracks if replaced a steel tendon with the same diameter. However, the deflection of the member was observed to be lower.
- Experimental results show that the value of Δf_{ps} depends on f_{pe}, f_{pu} and A_{ps} , while parameters such as f'_c and As do not affect fps significantly in hybrid beam.

The procedure presented in this research can be extended to the analysis of continuous members by considering the collapse mechanisms in each span and their plastic hinge locations. Further analysis is needed to verify its applicability

6.3. LCCA

This section presents a stochastic LCCA-based approach for finding the least expensive alternative at the project level and optimizing best project selection at the network level. A probabilistic multi-objective framework is proposed for conventional and innovative repair technologies for beams/girders. Project-level results show that the proposed new repair techniques for beams/girders with 10-year service life extension can save up to 15.1% in terms of agency cost and total life cycle cost (LCC) compare to the repair alternative using conventional concrete. For the proposed new repair techniques with 5-year service life extension, the cost benefits are relatively small (0.3% - 6.1%).

The network-level optimization model is formulated as a multi-choice, multi-dimensional knapsack problem and is solved by using an evolutionary algorithm, NSGA-II, to identify near-optimal solutions that balance the trade-offs between minimizing LCC and maximizing traffic loads of selected projects. Stochastic treatment of input parameters with high uncertainties provides us with a risk-based asset management approach that is more versatile and comprehensive than deterministic LCCA when it comes to making long-term decisions. In addition, clustering strategies are integrated into the decision process to enhance the traditional multi-objective LCCA by adding the capability of partitioning the pareto-optimal solutions based on additional preference. Two additional preference, maximizing available budget and maximizing network-level condition rating, are considered in the case study. The alternative that using FR-FC for girder repair and FR-SCC for rehabilitation with 10-year service life extension was found to be more sustainable than conventional repair technique on network-level as well. As an ongoing research effort, the proposed method will be further validated with more data from multiple states.

REFERENCES

- AASHTO. "AASHTO LRFD Selection of Girder Depth and Spacing." accessed June. http://bridgewiz.com/aashto-lrfd-selection-girder-depth-spacing/#toggle-id-2.
- Administration, Federal Highway. 1995. Recording and coding guide for the structure inventory and appraisal of the nation's bridges. US Dept. of Transportation Washington, DC.
- Allah Bukhsh, Zaharah, Irina Stipanovic, Giel Klanker, Alan O'Connor, and Andre G Doree. 2018. "Network level bridges maintenance planning using Multi-Attribute Utility Theory." Structure and Infrastructure Engineering:1-14.
- ASCE, 2017. 2017 infrastructure report card. Reston, VA: ASCE.
- Bai, Qiang, Anwaar Ahmed, Zongzhi Li, and Samuel Labi. 2015. "A Hybrid Pareto Frontier Generation Method for Trade-Off Analysis in Transportation Asset Management." Computer-Aided Civil and Infrastructure Engineering 30 (3):163-180.
- Barker, Michael. 2017. "Bridge Economy and Life Cycle Costs of Steel & Concrete Bridges." NACE 2017 Short Span Steel Bridge Workshop, Cincinnati, OH.
- Boatman, Brandon. 2010. "Prestressed vs. Steel Beams: Expected Service Life." Lansing: State of Michigan Department of Transportation.
- Bonstedt, Hank. 2010. "Life-cycle cost analysis for bridges–In search of better investment and engineering decisions." Proc., Pennsylvania Prestressed Concrete Association.
- Bryce, James, Samer Katicha, Gerardo Flintsch, Nadarajah Sivaneswaran, and Joño Santos. 2014. "Probabilistic Life-Cycle Assessment as Network-Level Evaluation Tool for Use and Maintenance Phases of Pavements." Transportation Research Record: Journal of the Transportation Research Board (2455):44-53.
- Deb, Kalyanmoy, Amrit Pratap, Sameer Agarwal, and TAMT Meyarivan. 2002. "A fast and elitist multiobjective genetic algorithm: NSGA-II." IEEE transactions on evolutionary computation 6 (2):182-197.
- Eamon, Christopher D, Elin A Jensen, Nabil F Grace, and Xiuwei Shi. 2012. "Life-cycle cost analysis of alternative reinforcement materials for bridge superstructures considering cost and maintenance uncertainties." Journal of Materials in Civil Engineering 24 (4):373-380.
- Federal Highway Administration. 2016. Federal Register 73196: Asset Management Plans and Periodic Evaluations of Facilities Repeatedly Requiring Repair and Reconstruction Due to Emergency Events.
- Federal Highway Administration. 2017. Using A Life Cycle Planning Process To Support Asset Management, Final Document.
- FHWA. 1998. Life-Cycle Cost Analysis Technical Bulletin.
- FHWA. 2002. Life-Cycle Cost Analysis Primer
- Gao, Jingqin, Kaan Ozbay, Hani Nassif, and Onur Kalan. "Stochastic Multi-Objective Optimization-Based Life Cycle Cost Analysis for New Construction Materials and Technologies." Transportation Research Record. doi: 10.1177/0361198119853578.
- Jawad, Dima J. 2003. "Life cycle cost optimization for infrastructure facilities (Ph.D. Dissertation)." Doctoral Thesis, Rutgers University.
- Liang, Ming-Te, Wen-Hu Tsao, Chi-Way Lin, and Wen-Lung Tsao. 2007. "Studies on the life-cycle cost analysis of existing prestressed concrete bridges." Journal of Marine Science and Technology 15 (3):247-254.

- Liu, Min, and Dan M Frangopol. 2005. "Balancing connectivity of deteriorating bridge networks and long-term maintenance cost through optimization." Journal of Bridge Engineering 10 (4):468-481.
- Mallela, Jagannath, and Suri Sadavisam. 2011. Work Zone Road User Costs: Concepts and Applications: US Department of Transportation, Federal Highway Administration.
- Marzouk, Mohamed, and Magdy Omar. 2013. "Multiobjective optimisation algorithm for sewer network rehabilitation." Structure and Infrastructure Engineering 9 (11):1094-1102.
- O. Swei, J. Gregory, and R. Kirchain. 2015. "Developing a Network-Level Pavement Management." accessed May. cshub.mit.edu/sites/default/files/documents/Final_OSwei_NetworkAssetMgmt_Issue9.pdf.
- Ozbay, K, O Yanmaz-Tuzel, S Mudigonda, B Bartin, and J Berechman. 2007. Cost of Transporting People in New Jersey-Phase II. New Jersey Department of Transportation Final Report. Report No FHWA/NJ-2007-003.
- Ozbay, Kaan, Bekir Bartin, Ozlem Yanmaz-Tuzel, and Joseph Berechman. 2007. "Alternative methods for estimating full marginal costs of highway transportation." Transportation Research Part A: Policy and Practice 41 (8):768-786.
- Ozbay, Kaan, and Pushkin Kachroo. 1999. Incident management in intelligent transportation systems. Norwood, MA: Artech House Publishers.
- Patidar, V, S Labi, KC Sinha, and PD Thompson. 2007. "NCHRP Report 590 - Multi-objective optimization for bridge management systems." Multiobjective Optimization for Bridge Management Systems.
- Patidar, Vandana. 2007. Multi-objective optimization for bridge management systems. Vol. 67: Transportation Research Board.
- Sinha, Kumares C, Samuel Labi, Bobby G McCullouch, Abhishek Bhargava, and Qiang Bai. 2009. "Updating and enhancing the Indiana bridge management system (IBMS)."
- Sobanjo, John O, and Paul D Thompson. 2007. Decision Support for Bridge Programming and Budgeting, Final Report.
- Wassef, Wagdy G, John M Kulicki, Hani Nassif, Dennis Mertz, and Andrzej S Nowak. 2014. "Calibration of AASHTO LRFD Concrete Bridge Design Specifications for Serviceability." NCHRP Web Document (201).
- Weyers, Richard E, Brian D Prowell, Michael M Sprinkel, and Michael Vorster. 1993. "Concrete bridge protection, repair, and rehabilitation relative to reinforcement corrosion: A methods application manual." Contract 100:103.
- Yeo, Hwasoo, Yoonjin Yoon, and Samer Madanat. 2010. "Maintenance optimization for heterogeneous infrastructure systems: Evolutionary algorithms for bottom-up methods." In Sustainable and Resilient Critical Infrastructure Systems, 185-199. Springer.
- Yu, Wei, Baizhan Li, Hongyuan Jia, Ming Zhang, and Di Wang. 2015. "Application of multi-objective genetic algorithm to optimize energy efficiency and thermal comfort in building design." Energy and Buildings 88:135-143.
- Zhang, Han, Gregory A Keoleian, and Michael D Lepech. 2012. "Network-level pavement asset management system integrated with life-cycle analysis and life-cycle optimization." Journal of infrastructure Systems 19 (1):99-107.